

# Joint Modeling of Anatomical and Functional Connectivity for Population Studies

Archana Venkataraman\*, Yogesh Rathi, Marek Kubicki, Carl-Fredrik Westin, and Polina Golland

**Abstract**—We propose a novel probabilistic framework to merge information from diffusion weighted imaging tractography and resting-state functional magnetic resonance imaging correlations to identify connectivity patterns in the brain. In particular, we model the interaction between *latent* anatomical and functional connectivity and present an intuitive extension to population studies. We employ the EM algorithm to estimate the model parameters by maximizing the data likelihood. The method simultaneously infers the templates of latent connectivity for each population and the differences in connectivity between the groups. We demonstrate our method on a schizophrenia study. Our model identifies significant increases in functional connectivity between the parietal/posterior cingulate region and the frontal lobe and reduced functional connectivity between the parietal/posterior cingulate region and the temporal lobe in schizophrenia. We further establish that our model learns predictive differences between the control and clinical populations, and that combining the two modalities yields better results than considering each one in isolation.

**Index Terms**—Biomedical imaging, brain modeling, magnetic resonance imaging (MRI), population analysis.

## I. INTRODUCTION

THE INTERACTION between anatomical and functional imaging modalities offers a rich framework for understanding the effects of neuropsychiatric disorders. Specifically, correlations present in resting-state functional magnetic resonance imaging (fMRI) data are believed to reflect the intrinsic functional connectivity of the brain [1], [2]. Similarly, diffusion weighted imaging (DWI) tractography is used to estimate the underlying white matter fibers and provides valuable information about anatomical connectivity within the brain [3]. To date, relatively little progress has been made on combining informa-

tion from these imaging modalities. Prior analysis has focused on correspondences between independently computed statistics of fMRI and DWI data [4]–[7]. Clinical studies typically identify significant population differences separately within each modality and compare them *a posteriori* [8], [9].

In this work, we propose and demonstrate a novel probabilistic framework to infer the relationship between resting-state fMRI and DWI tractography. In particular, we introduce the notion of *latent* anatomical and functional connectivity between brain regions. These variables represent an underlying process in the brain which cannot be observed directly from the data. The resulting model describes how the latent connectivity differs between two populations and makes intuitive assumptions about the fMRI and DWI image generation process to construct the data likelihood. Our fMRI/DWI observation model is shared across subjects. Hence, we assume that the effects of a disorder can be explained via changes in latent anatomical and functional connectivity. To the best of our knowledge, ours is the first stochastic model to combine resting-state fMRI and DWI data in order to infer changes induced by a neurological disease.

We employ the EM algorithm to efficiently estimate templates of latent connectivity for each population and to identify group differences. The EM algorithm optimizes the model parameters by maximizing the data likelihood. We employ permutation tests and cross validation to verify the robustness of our method. We perform an extensive evaluation of the model on synthetic data. In addition, we learn stable patterns of interaction in a population study of schizophrenia.

Schizophrenia is a poorly-understood disorder marked by widespread cognitive difficulties affecting intelligence, memory, and executive attention. These impairments are not localized to a particular cortical region, but rather, they reflect abnormalities in widely-distributed functional and anatomical networks [10], [11]. Accordingly, our model identifies connectivity differences dispersed throughout the brain. This paper extends our prior work presented at the International Conference on Medical Image Computing and Computer Assisted Intervention [12] by providing more detailed derivations of the model and estimation procedure and by including more experimental evaluation of the methods.

The remainder of this paper is organized as follows. Section II summarizes prior research on joint modeling of fMRI and DWI data. We also review clinical findings of schizophrenia in this section. We introduce our generative model in Section III and develop the corresponding inference algorithm in Section IV. Section V presents the framework used for the empirical validation of our approach. Sections VI and VII report experimental results based on synthetic and clinical data, respectively.

Manuscript received June 16, 2011; revised August 11, 2011; accepted August 15, 2011. Date of publication August 30, 2011; date of current version February 03, 2012. This work was supported in part by the National Alliance for Medical Image Analysis (NIH NIBIB NAMD U54-EB005149), in part by the Neuroimaging Analysis Center (NIH NCRR NAC P41-RR13218), in part by the NSF CAREER Grant 0642971, and in part by NIH R01MH074794. A. Venkataraman was supported by the National Defense Science and Engineering Graduate Fellowship (NDSEG). *Asterisk indicates corresponding author.*

\*A. Venkataraman is with the Computer Science and Artificial Intelligence Laboratory, Massachusetts Institute of Technology, Cambridge, MA 02139 USA.

C.-F. Westin is with the Computer Science and Artificial Intelligence Laboratory, Massachusetts Institute of Technology, Cambridge, MA 02139 USA and also with the Laboratory for Mathematics Imaging, Harvard Medical School, Boston, MA 02215 USA.

Y. Rathi and M. Kubicki are with the Psychiatry Neuroimaging Laboratory, Harvard Medical School, Boston, MA 02215 USA.

P. Golland is with the Computer Science and Artificial Intelligence Laboratory, Massachusetts Institute of Technology, Cambridge, MA 02139 USA.

Digital Object Identifier 10.1109/TMI.2011.2166083

Section VIII discusses the behavior of our model, its advantages and drawbacks, and future directions of research. We conclude with a summary of contributions in Section IX.

## II. BACKGROUND AND RELATED WORK

### A. Multimodal Analysis in the Brain

Both DWI and fMRI have recently gained popularity as non-invasive imaging tools useful for the study of the brain and the effects of neurological diseases. DWI captures the anisotropic diffusion of water throughout the brain and is often used to estimate white matter bundles via tractography. Common measures of anatomical connectivity include the probability of diffusion between two brain regions, the number of fibers linking two regions, and the mean fractional anisotropy (FA) along the tracts [3]. fMRI studies can be divided into two broad categories. *Task-based* studies measure the response to a given experimental paradigm in order to localize brain functionality [13]. In contrast, *resting-state* fMRI measures spontaneous, low-frequency oscillations. Correlations within these signals reflect the intrinsic functional connectivity between brain regions [1], [2].

Early work in multimodal analysis focused on the relationship between task fMRI activations and the underlying anatomy. One popular technique is to use regions of fMRI activation as seed points for tractography [14]–[16]. Another approach is to quantify the relationship between anatomical connectivity and measures of functional co-activation in predefined regions of interest [17], [18].

Presently, the focus has shifted to resting-state fMRI for joint analysis [19]. Studies commonly compute statistics of the fMRI and DWI signals (such as fMRI correlations, fractional anisotropy values, etc.) and search for correspondences between these metrics *a posteriori* [4], [5], [20]. A notable exception is the recently demonstrated approach in [6] where the authors construct cortical connection graphs based on histological data of the macaw brain and simulate the corresponding functional correlations using a dynamical system to model the interactions within the graph. Although promising, this analysis has not been replicated using DWI data in humans.

The above methods have yielded many insights into the nature of connectivity in the brain. For example, fMRI-guided tractography has improved the mapping of the motor, visual and language areas [14]–[16]. It has also been established that while a high degree of anatomical connectivity predicts higher functional correlations, the converse does not always hold [4], [20]. For example, strong functional correlations can be found between spatially distributed locations in the brain, whereas one is more likely to identify white matter tracts connecting nearby regions.

The main limitation of the prior works in joint fMRI/DWI modeling is an artificial separation between the modalities. The analysis is largely performed on the individual modalities, and information is later pooled into a joint representation. In contrast, we assume that the structure and organization of the brain is captured by some underlying generative process. The fMRI

and DWI measures are *conditionally independent* given the details of this latent process. We use *both* modalities to infer population templates of connectivity and demonstrate that our model captures stable patterns of connectivity.

### B. Population Studies

Univariate tests and random effects analysis are, to a great extent, the standard in population studies of connectivity [21]–[24]. In this case, significantly different connections are identified using a statistical score that is computed independently for each functional correlation or DWI measure.

Prior work has also explored multi-pattern analysis for functional connectivity. Specifically, group independent component analysis (gICA) has been used to represent the data as a set of spatially-independent regions with associated time courses [25], [26]. In [25], group functional connectivity is computed as the maximum lagged correlation between the detected time courses, and two-sample t-tests are employed to identify significant population differences. In [26], a neural network is constructed for patient classification of first-episode schizophrenia.

Our work focuses on a population study of schizophrenia, as several of its clinical symptoms may be linked to aberrations in connectivity [27]. Relatively few studies to date have combined resting-state fMRI and DWI tractography to analyze schizophrenia [8], [9]. Univariate statistical tests are commonly used to identify significant population differences in both temporal correlations and in mean Fractional Anisotropy (FA) values. The relevant connections are then compared across modalities. This approach treats functional and structural connections as independent and ignores distributed patterns of connectivity. In contrast, we jointly infer the network of functional and anatomical connectivity.

### C. Schizophrenia: Findings and Hypotheses

Schizophrenia is a neuropsychiatric disorder characterized by gross distortions in the perception of reality. Despite generating considerable interest in the neuroscience community, the origins and expression of the disease are still poorly understood [28]. For example, structural findings only weakly and inconsistently correlate with the clinical and cognitive symptoms of schizophrenia [29]. Similarly, functional experiments report deficits in many cognitive domains, most notably memory and attention, but do not consistently report clinical correlates [30].

At present, the cognitive impairments of schizophrenia are believed to reflect underlying abnormalities in distributed brain networks. In particular, schizophrenia may compromise neural communication between cortical regions [27]. Recent studies have also focused on the degeneration of anatomical connectivity [24], fueled in part by postmortem and genetic evidence of myelination anomalies in patients with schizophrenia.

Findings from resting-state fMRI data include reduced connectivity in the brain's default network [31], [32], dorso-lateral prefrontal cortex [23] and a widespread reduction in connectivity throughout the brain [22]. In contrast, although the majority of DWI studies report white matter abnormalities, there is no consensus on the location and nature of these changes [24], [33]. The most commonly reported anomalies are between frontal and temporal lobes and between the

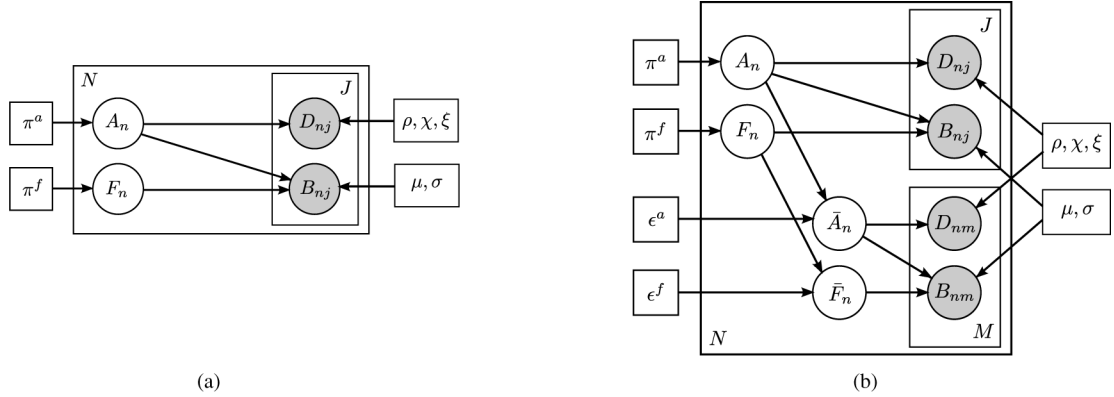


Fig. 1. (a) Joint connectivity model for a single population. The pairwise connections are indexed with  $n = 1, \dots, N$ .  $A_n$  represents the latent anatomical connectivity of the  $n$ th connection, and  $F_n$  denotes the corresponding latent functional connectivity.  $D_{nj}$  and  $B_{nj}$  are the observed DWI and fMRI measurements, respectively, for the  $n$ th connection in the  $j$ th subject. Squares indicate nonrandom parameters; circles indicate random variables; observed variables are shaded. (b) Joint model for the effects of schizophrenia. The control population is generated according to the model in (a). The schizophrenia templates are identified by an overbar, and the subjects are indexed by  $m = 1, \dots, M$ . (a) Joint fMRI/DWI model. (b) Model of population differences.

TABLE I  
RANDOM VARIABLES (TOP) AND NONRANDOM PARAMETERS (BOTTOM) IN OUR GRAPHICAL MODEL SHOWN IN FIG. 1

$A_n$	Latent anatomical connectivity for the $n$ th connection in the control population
$\bar{A}_n$	Latent anatomical connectivity for the $n$ th connection in the schizophrenia population
$F_n$	Latent functional connectivity for the $n$ th connection in the control population
$\bar{F}_n$	Latent functional connectivity for the $n$ th connection in the schizophrenia population
$D_{nj}$	Observed DWI measure for connection $n$ in subject $j$
$B_{nj}$	Observed fMRI measure for connection $n$ in subject $j$
$\pi^a$	Prior for binary anatomical connectivity $A_n$
$\pi^f$	Prior for multinomial functional connectivity $F_n$
$\epsilon^a$	Probability of change in anatomical connectivity
$\epsilon^f$	Probability of change in functional connectivity
$\rho_i$	Probability of failing to find a white matter tract given that $A_n = i$ ( $i = 0, 1$ )
$\chi_i$	Mean DWI value if there is a white matter tract given that $A_n = i$ ( $i = 0, 1$ )
$\xi_i^2$	Variance of DWI values if there is a white matter tract given that $A_n = i$ ( $i = 0, 1$ )
$\mu_{ik}$	Mean fMRI value given that $A_n = i$ and $F_n = k$ ( $i = 0, 1, k = -1, 0, 1$ )
$\sigma_{ik}^2$	Variance of fMRI values given that $A_n = i$ and $F_n = k$ ( $i = 0, 1, k = -1, 0, 1$ )

hemispheres [24]. They are believed to reflect the underlying neurodevelopmental or neurodegenerative processes affecting myelinated axons. Since DWI tractography and resting-state fMRI data provide different information about the underlying structure and dynamics of the brain, we believe that joint analysis of these modalities will improve our understanding of brain connectivity and of the effects that diseases such as schizophrenia have on the connectivity pattern. Additionally, resting-state fMRI is particularly attractive for clinical populations, since patients are not required to perform challenging experimental paradigms.

To summarize, prior work in joint analysis of anatomical and functional connectivity has focused on correspondences rather than the interaction between fMRI and DWI data. This type of analysis has produced widely varied results in the study of schizophrenia. In the next section, we present a novel framework for multimodal analysis that allows us to infer the patterns of connectivity and the changes induced by a disorder.

### III. GENERATIVE MODEL

We combine the DWI tractography and fMRI correlations in a unified generative model of the brain. In particular, *latent*

anatomical and functional connectivity specify a template organization of the brain for a given population. Anatomical connectivity indicates whether or not there are any white matter fiber bundles between two regions. It does not quantify the number or trajectory of these fibers. Functional connectivity describes how two regions co-activate (positive relationship, negative relationship or no relationship). We do not have access to these “ground truth” variables. Rather, we observe noisy measurements via DWI tractography and resting-state fMRI correlations. Although DWI and fMRI signals vary across subjects, we assume they are generated probabilistically from a common latent template.

We first develop the probabilistic framework within a control population. This formulation serves as a foundation for modeling group differences, presented later in the section.

#### A. Single Population Model

Fig. 1(a) depicts our model for a single population, and Table I summarizes our notation. The individual subject data is generated from the latent population templates of connectivity. All latent and observed variables are generated independently for each pairwise connection; the data likelihood parameters are shared across connections.

a) *Prior*: Let  $N$  be the total number of relevant connections in the brain. We use  $A_n$  and  $F_n$  to denote the latent anatomical and functional connectivity indicators between the two regions associated with the  $n$ th connection ( $1 \leq n \leq N$ ). The anatomical connectivity  $A_n$  indicates the presence or absence of a *direct* anatomical pathway between two regions. We model  $A_n$  as a binary random variable. The scalar parameter  $\pi^a$  specifies the *a priori* probability that a connection is present

$$P(A_n; \pi^a) = (\pi^a)^{A_n} (1 - \pi^a)^{1 - A_n}. \quad (1)$$

In contrast, the functional connectivity  $F_n$  is a tri-state random variable. These states represent 1) little or no functional co-activation ( $F_n = 0$ ), 2) positive functional synchrony ( $F_n = 1$ ), and 3) negative functional synchrony ( $F_n = -1$ ) between two regions. Strong negative correlations are often found in resting-state fMRI data. Since there is no consensus about their origin and significance [34], we isolate negative connectivity as a separate category. For notational convenience, we represent  $F_n$  as a length-three indicator vector  $F_n = [F_{n,-1} \ F_{n,0} \ F_{n,1}]^T$  with exactly one of its elements equal to one

$$P(F_n; \pi^f) = \prod_{k=-1}^1 (\pi_k^f)^{F_{n,k}} \quad (2)$$

where  $\pi_k^f$  is the probability that the  $n$ th functional connection is assigned to state  $k$ .

Although we model latent connectivity via discrete random variables, the posterior probability distributions of the variables  $\{A_n, F_n\}$  provide a natural measure of connection strength. These distributions form the basis for subsequent analysis in the population studies.

Below, we describe how the latent connectivity templates affect the observed measures in individual subjects. Empirically, we observe that the variability of the DWI and fMRI measures of connectivity across connections and across subjects can be reasonably approximated using Gaussian distributions (Section VII-B provides more details). It is not surprising since both measures are computed as averages of the observed image data and should therefore approach Gaussian distributions as the number of elements increases. Moreover, using Gaussian likelihoods for the observed data greatly simplifies the learning/inference algorithm and allows for efficient fitting of the model parameters.

b) *DWI Likelihood*: Let  $J$  be the number of subjects. The DWI measurement  $D_{nj}$  for the  $j$ th subject is a noisy observation of the anatomical connectivity  $A_n$ . In this work we use the average FA along white matter fibers to assess DWI connectivity. The model can be readily extended to accommodate other measures of connectivity by redefining the data likelihood term.

Our observation model for  $D_{nj}$  explicitly accounts for errors in tractography. These include missing tracts between anatomically connected regions and spurious tracts between isolated ones. In particular, if tractography identifies one or more white matter fibers between two regions, the value of  $D_{nj}$  is modeled

as a Gaussian random variable whose mean and variance depend on the anatomical connectivity indicator  $A_n$ . Otherwise,  $D_{nj}$  is set to zero. Mathematically

$$P(D_{nj} | A_n = i; \{\rho, \chi, \xi\}) = \rho_i \delta(D_{nj}) + (1 - \rho_i) \mathcal{N}(D_{nj}; \chi_i, \xi_i^2) \quad (3)$$

where  $\delta(\cdot)$  is the Dirac delta function and  $\mathcal{N}(\cdot; \chi, \xi^2)$  denotes a Gaussian distribution with mean  $\chi$  and variance  $\xi^2$ .  $\rho_0, \rho_1$  are the probability of failing to find a white matter tract between the regions in the absence ( $A_n = 0$ ) or presence ( $A_n = 1$ ) of a latent anatomical connection, respectively. Ideally,  $\rho_0 = 1$  and  $\rho_1 = 0$ , i.e., a white matter tract should be found if and only if there is an underlying anatomical connection. However, detection via tractography is imperfect. In practice  $D_{nj}$  is strictly positive if a tract is found between the regions, and the Gaussian distribution in (3) adequately captures the data variation as our results in Section VII-B suggest.

1) *fMRI Likelihood*: We model the BOLD fMRI correlation  $B_{nj}$  for connection  $n$  of the  $j$ th subject as a Gaussian random variable whose mean and variance depend on *both* the latent functional connectivity  $F_n$  and anatomical connectivity  $A_n$ . This reflects the finding that direct anatomical connections predict higher functional correlations [4], [5]

$$P(B_{nj} | A_n = i, F_n = k; \{\mu, \sigma\}) = \mathcal{N}(B_{nj}; \mu_{ik}, \sigma_{ik}^2). \quad (4)$$

In this work, we compute  $B_{nj}$  using Pearson correlation coefficients. Once again, our empirical analysis in Section VII-B suggests that the Gaussian likelihood in (4) provides a reasonable approximation for the data distribution.

Combining all the elements of the model in (1)–(4), we obtain the joint log-likelihood of all hidden and observed variables for the  $n$ th connection

$$\begin{aligned} \log P(A_n, F_n, \mathbf{D}_n, \mathbf{B}_n; \{\pi, \mu, \sigma^2, \rho, \chi, \xi^2\}) &= A_n \log(\pi^a) + (1 - A_n) \log(1 - \pi^a) + \sum_{k=-1}^1 F_{n,k} \log(\pi_k^f) \\ &+ \sum_{j=1}^J [(1 - A_n) \log(\rho_0 \delta(D_{nj}) + (1 - \rho_0) \mathcal{N}(D_{nj}; \chi_0, \xi_0^2))] \\ &+ \sum_{j=1}^J [A_n \log(\rho_1 \delta(D_{nj}) + (1 - \rho_1) \mathcal{N}(D_{nj}; \chi_1, \xi_1^2))] \\ &+ \sum_{j=1}^J \sum_{k=-1}^1 [(1 - A_n) F_{n,k} \log \mathcal{N}(B_{nj}; \mu_{0k}, \sigma_{0k}^2)] \\ &+ \sum_{j=1}^J \sum_{k=-1}^1 [A_n F_{n,k} \log \mathcal{N}(B_{nj}; \mu_{1k}, \sigma_{1k}^2)]. \end{aligned} \quad (5)$$

## B. Population Differences

Fig. 1(b) presents an extension of our model to a population study involving controls and schizophrenia patients. We assume that the differences between the groups are explained entirely

by changes in latent connectivity and that the two populations share the same data likelihood model.

In particular, we assume the model in Fig. 1(a) for the control population and treat the latent connectivity template  $\{\bar{A}_n, \bar{F}_n\}$  of the schizophrenia population as a ‘‘corrupted’’ version of the healthy template. In particular, with (small) probability, each connection can switch its state

$$P(\bar{A}_n | A_n; \epsilon^a) = (\epsilon^a)^{A_n(1-\bar{A}_n)+(1-A_n)\bar{A}_n} \cdot (1 - \epsilon^a)^{A_n\bar{A}_n+(1-A_n)(1-\bar{A}_n)} \quad (6)$$

$$P(\bar{F}_n | F_n; \epsilon^f) = \left(\frac{\epsilon^f}{2}\right)^{(1-F_n^T \bar{F}_n)} (1 - \epsilon^f)^{F_n^T \bar{F}_n}. \quad (7)$$

Rather than parameterizing all possible connectivity differences, we rely on scalars  $\epsilon^a$  and  $\epsilon^f$  to govern the probability of change within each modality. For binary random variables  $A_n$  and  $\bar{A}_n$ , this implies that the probability of change in anatomical connectivity does not depend on the value of  $A_n$ . A similar property holds for the tri-state random variables  $F_n$  and  $\bar{F}_n$ . Additionally, (7) assumes that functional connectivity switches to its other two states with equal probability. Empirically, our results are more robust using (6) and (7) than if we infer all transition probabilities for each modality.

#### IV. ALGORITHMS

We employ the maximum likelihood (ML) framework to estimate the model parameters

$$\begin{aligned} \hat{\Theta}^* &= \underset{\Theta}{\operatorname{argmax}} \sum_{n=1}^N \log P(\mathbf{D}_n, \mathbf{B}_n; \Theta) \\ &= \underset{\Theta}{\operatorname{argmax}} \sum_{n=1}^N \log \sum_{A_n, F_n} P(A_n, F_n, \mathbf{D}_n, \mathbf{B}_n; \Theta) \end{aligned} \quad (8)$$

where  $\Theta$  is the set of model parameters.  $\Theta = \{\pi, \mu, \sigma^2, \rho, \chi, \xi^2\}$  for the single-population model;  $\Theta = \{\pi, \mu, \sigma^2, \rho, \chi, \xi^2, \epsilon\}$  for the model of population differences.

We derive the expectation-maximization (EM) algorithm [35] for fitting the models. The EM algorithm constructs the joint posterior of all hidden variables, which is later used to infer population differences. The total number of model parameters is small. In particular, the posterior distribution can be computed directly from the observed data and the model parameters  $\{\pi, \mu, \sigma^2, \rho, \chi, \xi^2, \epsilon\}$ . Since these parameters are shared across connections and across subjects, the solution is based on a small set of unknown values.

##### A. Single Population Model

We use  $\mathbf{X}_n = \{A_n, F_n\}$  and  $\mathbf{Y}_n = \{\mathbf{D}_n, \mathbf{B}_n\}$  to denote the hidden and observed variables, respectively, associated with the  $n$ th connection.

Since  $A_n$  is a binary random variable and  $F_n$  is a tri-state random variable, the latent vector  $\mathbf{X}_n$  assumes one of six distinct values. The EM algorithm iterates between estimating the posterior probability of the hidden variables  $\mathbf{X}_n$  and estimating

the model parameters  $\Theta$ . Due to the independence of pairwise connections, this problem reduces to a standard mixture model with six components.

For notational simplicity, we index the six states of  $\mathbf{X}_n$  using a set  $\{1, \dots, 6\}$ . We construct the associated prior distribution  $P(\mathbf{X}_n = l; \Theta)$  and data likelihood  $P(\mathbf{Y}_n | \mathbf{X}_n = l; \Theta)$  by evaluating (1)–(4). In particular, if the index  $l$  denotes the latent assignment  $A_n = i, F_n = k$

$$P(\mathbf{X}_n = l; \Theta) = (\pi^a)^i (1 - \pi^a)^{(1-i)} \cdot \pi_k^f$$

$$\begin{aligned} P(\mathbf{Y}_n | \mathbf{X}_n = l; \Theta) &= \prod_{j=1}^J [\rho_i \delta(D_{nj}) \\ &+ (1 - \rho_i) \mathcal{N}(D_{nj}; \chi_i, \xi_i^2)] \mathcal{N}(B_{nj}; \mu_{ik}, \sigma_{ik}^2). \end{aligned}$$

Independence across pairwise connections gives rise to a simple sum in the log-likelihood of the observed and hidden variables

$$\mathcal{L}(\mathbf{X}, \mathbf{Y}; \Theta) = \sum_{n=1}^N \log P(\mathbf{X}_n; \Theta) P(\mathbf{Y}_n | \mathbf{X}_n; \Theta). \quad (9)$$

**E-Step:** We fix the model parameter estimates  $\hat{\Theta}$  and update the posterior probability estimates  $\hat{p}_{nl}$  of the latent variables

$$\begin{aligned} \hat{p}_{nl} &= P(\mathbf{X}_n = l | \mathbf{Y}_n; \hat{\Theta}) \\ &\propto P(\mathbf{X}_n = l; \hat{\Theta}) P(\mathbf{Y}_n | \mathbf{X}_n = l; \hat{\Theta}) \\ \text{s.t. } &\sum_{l=1}^6 \hat{p}_{nl} = 1. \end{aligned} \quad (10)$$

**M-Step:** We fix the posterior probability estimates  $\hat{p}_{nl}$  and update the model parameter estimates  $\hat{\Theta}$ . Given a guess of the parameters  $\hat{\Theta}$  from the previous iteration, we construct a lower bound to the log-likelihood  $\Psi(\Theta, \hat{\Theta}) = E_{\mathbf{X} | \mathbf{Y}}[\log P(\mathbf{X}, \mathbf{Y}; \Theta) | \mathbf{Y}, \hat{\Theta}]$ . With some algebraic manipulation, we obtain

$$\begin{aligned} \Psi(\Theta, \hat{\Theta}) &= \sum_{l=1}^6 \sum_{n=1}^N \hat{p}_{nl} \log [P(\mathbf{X}_n = l; \Theta) P(\mathbf{Y}_n | \mathbf{X}_n = l; \Theta)]. \end{aligned} \quad (11)$$

The parameter updates are obtained by differentiating (11) with respect to  $\Theta$  and setting the gradient equal to zero. For notational convenience, we let  $J_n^0$  be the number of subjects for which  $D_{nj} = 0$  (i.e., no tract was detected). The binomial and multinomial priors reduce to intuitive sums of the latent posterior probability estimates

$$\hat{\pi}^a = \frac{1}{N} \sum_{n=1}^N \sum_{l: A_n=i} \hat{p}_{nl} \quad \hat{\pi}_k^f = \frac{1}{N} \sum_{n=1}^N \sum_{l: F_n=k} \hat{p}_{nl}. \quad (12)$$

The probability  $\rho$  is the empirical likelihood of not finding a white matter tract between two regions

$$\hat{\rho}_i = \frac{\sum_{n=1}^N J_n^0 \sum_{l: A_n=i} \hat{p}_{nl}}{\sum_{n=1}^N J \sum_{l: A_n=i} \hat{p}_{nl}}. \quad (13)$$

TABLE II  
LIKELIHOOD PARAMETER UPDATES FOR THE MODEL OF POPULATION DIFFERENCES

$$\begin{aligned}\hat{\mu}_{ik} &= \frac{\sum_{n=1}^N \left[ \sum_{j=1}^J B_{nj} \sum_{l:A_n=i, F_{nk}=1} \hat{p}_{nl} + \sum_{m=1}^M B_{nm} \sum_{l:\bar{A}_n=i, \bar{F}_{nk}=1} \hat{p}_{nl} \right]}{\sum_{n=1}^N \left[ J \sum_{l:A_n=i, F_{nk}=1} \hat{p}_{nl} + M \sum_{l:\bar{A}_n=i, \bar{F}_{nk}=1} \hat{p}_{nl} \right]} \\ \hat{\sigma}_{ik}^2 &= \frac{\sum_{n=1}^N \left[ \sum_{j=1}^J (B_{nj} - \mu_{ik})^2 \sum_{l:A_n=i, F_{nk}=1} \hat{p}_{nl} + \sum_{m=1}^M (B_{nm} - \mu_{ik})^2 \sum_{l:\bar{A}_n=i, \bar{F}_{nk}=1} \hat{p}_{nl} \right]}{\sum_{n=1}^N \left[ J \sum_{l:A_n=i, F_{nk}=1} \hat{p}_{nl} + M \sum_{l:\bar{A}_n=i, \bar{F}_{nk}=1} \hat{p}_{nl} \right]} \\ \hat{\rho}_i &= \frac{\sum_{n=1}^N \left[ J_n^0 \sum_{l:A_n=i} \hat{p}_{nl} + M_n^0 \sum_{l:\bar{A}_n=i} \hat{p}_{nl} \right]}{\sum_{n=1}^N \left[ J \sum_{l:A_n=i} \hat{p}_{nl} + M \sum_{l:\bar{A}_n=i} \hat{p}_{nl} \right]} \\ \hat{\chi}_i &= \frac{\sum_{n=1}^N \left[ \sum_{j:D_{nj}>0} D_{nj} \sum_{l:A_n=i} \hat{p}_{nl} + \sum_{m:D_{nm}>0} D_{nm} \sum_{l:\bar{A}_n=i} \hat{p}_{nl} \right]}{\sum_{n=1}^N \left[ (J - J_n^0) \sum_{l:A_n=i} \hat{p}_{nl} + (M - M_n^0) \sum_{l:\bar{A}_n=i} \hat{p}_{nl} \right]} \\ \hat{\xi}_i^2 &= \frac{\sum_{n=1}^N \left[ \sum_{j:D_{nj}>0} (D_{nj} - \chi_i)^2 \sum_{l:A_n=i} \hat{p}_{nl} + \sum_{m:D_{nm}>0} (D_{nm} - \chi_i)^2 \sum_{l:\bar{A}_n=i} \hat{p}_{nl} \right]}{\sum_{n=1}^N \left[ (J - J_n^0) \sum_{l:A_n=i} \hat{p}_{nl} + (M - M_n^0) \sum_{l:\bar{A}_n=i} \hat{p}_{nl} \right]}\end{aligned}$$

The Gaussian likelihood parameters for the DWI measurements  $\mathbf{D}_n$  are given by the weighted empirical mean and empirical variance over all *nonzero* values

$$\hat{\chi}_i = \frac{\sum_{n=1}^N \sum_{j:D_{nj}>0} \frac{D_{nj}}{D_{nj}} \sum_{l:A_n=i} \hat{p}_{nl}}{\sum_{n=1}^N (J - J_n^0) \sum_{l:A_n=i} \hat{p}_{nl}} \quad (14)$$

$$\hat{\xi}_i^2 = \frac{\sum_{n=1}^N \sum_{j:D_{nj}>0} \frac{(D_{nj} - \chi_i)^2}{(D_{nj} - \chi_i)^2} \sum_{l:A_n=i} \hat{p}_{nl}}{\sum_{n=1}^N (J - J_n^0) \sum_{l:A_n=i} \hat{p}_{nl}}. \quad (15)$$

The likelihood parameters for the functional observations  $\mathbf{B}_n$  are similarly constructed as weighted statistics of the data

$$\hat{\mu}_{ik} = \frac{\sum_{n=1}^N \sum_{j=1}^J B_{nj} \sum_{l:A_n=i, F_{nk}=1} \hat{p}_{nl}}{J \sum_{n=1}^N \sum_{l:A_n=i, F_{nk}=1} \hat{p}_{nl}} \quad (16)$$

$$\hat{\sigma}_{ik}^2 = \frac{\sum_{n=1}^N \sum_{j=1}^J (B_{nj} - \mu_{ik})^2 \sum_{l:A_n=i, F_{nk}=1} \hat{p}_{nl}}{J \sum_{n=1}^N \sum_{l:A_n=i, F_{nk}=1} \hat{p}_{nl}}. \quad (17)$$

## B. Modeling Population Differences

The algorithm presented above can be easily extended to the two-population model in Fig. 1(b). This complete model is the primary focus of our work in the following sections. Below, we let  $\mathbf{X}_n = \{A_n, F_n, \bar{A}_n, \bar{F}_n\}$  and  $\mathbf{Y}_n = \{D_{nj}, B_{nj}, D_{nm}, B_{nm}\}$  denote the hidden and observed variables, respectively, of the  $n$ th pairwise connection.

Both  $A_n$  and  $\bar{A}_n$  are binary random variables and both  $F_n$  and  $\bar{F}_n$  are tri-state random variables. Therefore, the latent vector  $\mathbf{X}_n$  assumes one of 36 distinct values. Once again, we index the latent states of  $\mathbf{X}_n$  using  $l \in \{1, \dots, 36\}$  and map the estimation problem to the standard mixture model with 36 components.

**E-Step:** We construct the full prior and likelihood distributions  $P(\mathbf{X}_n = l; \Theta)$  and data likelihood  $P(\mathbf{Y}_n | \mathbf{X}_n = l; \Theta)$  using (1)–(7). The posterior estimate  $\hat{p}_{nl}$  is computed analogously to (10) for each value of  $(n, l)$ .

**M-Step:** As in the preceding section, we let  $J_n^0$  be the number of control subjects for whom  $D_{nj} = 0$  and  $M_n^0$  be the number of schizophrenia patients for whom  $D_{nm} = 0$ .

Once again, the probability estimates are intuitive sums of the latent posteriors. In this case, we must also solve for the parameters  $e^a, e^f$  in (6) and (7)

$$\hat{\pi}^a = \frac{1}{N} \sum_{n=1}^N \sum_{l:A_n=i} \hat{p}_{nl}, \quad \hat{\pi}_k^f = \frac{1}{N} \sum_{n=1}^N \sum_{l:F_{nk}=1} \hat{p}_{nl} \quad (18)$$

$$\hat{e}^a = \frac{1}{N} \sum_{n=1}^N \sum_{l:A_n \neq \bar{A}_n} \hat{p}_{nl}, \quad \hat{e}^f = \frac{1}{N} \sum_{n=1}^N \sum_{l:F_n \neq \bar{F}_n} \hat{p}_{nl}. \quad (19)$$

Since both populations share the same data likelihood model, the updates for  $\{\hat{\mu}, \hat{\sigma}^2, \hat{\rho}, \hat{\chi}, \hat{\xi}^2\}$  are derived from (13)–(17) by incorporating one data term for each population. These update equations are presented in Table II.

To summarize, we have presented the EM algorithm for both models in Fig. 1. The parameter updates are intuitive in both cases. The posterior distributions over the latent connectivity variables play a crucial role in the clinical application of our model as follows.

## C. Quantifying Group Differences

We assume that group differences are expressed in the latent templates  $\{A_n, F_n, \bar{A}_n, \bar{F}_n\}$ . Therefore, the main quantity of interest is the probability of change in the anatomical or functional connectivity templates for a given pairwise connection. We let  $\hat{e}_n^a$  denote the probability of a change in the anatomical connectivity for the  $n$ th connection, and we let  $\hat{e}_n^f$  denote the corresponding probability of change in functional connectivity. We estimate these values based on the inferred posterior probabilities  $\{\hat{p}_{nl}\}$

$$\hat{e}_n^a = \sum_{l:A_n \neq \bar{A}_n} \hat{p}_{nl}, \quad \hat{e}_n^f = \sum_{l:F_n \neq \bar{F}_n} \hat{p}_{nl}. \quad (20)$$

These values are the main output of our algorithm in the context of population studies.

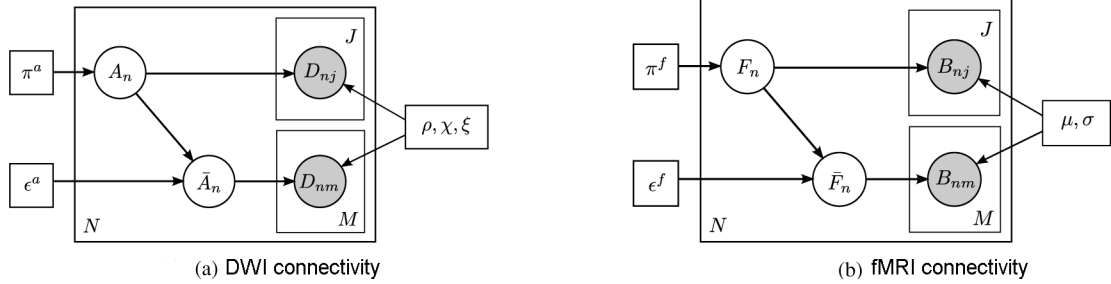


Fig. 2. Baseline models of population differences for a single modality. Once again, the pairwise connections are indexed with  $n = 1, \dots, N$ .  $A_n$  represents the latent anatomical connectivity of the  $n$ th connection, and  $F_n$  denotes the corresponding latent functional connectivity.  $D_{nj}$  and  $B_{nj}$  are the observed DWI and fMRI measurements, respectively, for the  $n$ th connection in the  $j$ th subject. The schizophrenia templates are identified by an overbar, and the subjects are indexed by  $m = 1, \dots, M$ . Squares indicate non-random parameters; circles indicate random variables; observed variables are shaded. The variables, parameters and likelihood of (a) remains unchanged from the joint model. The likelihood in (b) is modified to reflect only the three functional connectivity states. (a) DWI-only Model, (b) fMRI-only Model.

## V. MODEL EVALUATION

### A. Model Significance

Although our model is based on standard probability distributions (Gaussian and multinomial), the joint distribution is not Gaussian due to multiplicative interactions and the effects of unknown nonrandom parameters. Therefore, we evaluate significance through nonparametric permutation tests. Specifically, we construct the distribution of these values under the null hypothesis by randomly permuting the subject labels (NC versus SZ) 10 000 times. For each permutation, we fit the model and compute the relevant statistics  $\hat{\epsilon}_n^a, \hat{\epsilon}_n^f$ . The significance (p-value) of each connection is equal to the proportion of permutations for which the computed statistic is greater than or equal to the value obtained under the true labeling.

### B. Classification Accuracy

We also quantify the model's predictive power via ten-fold cross validation. We randomly divide the subjects into 10 groups, each with an equal number of controls and schizophrenia patients.<sup>1</sup> We fit the model using nine training groups and employ a likelihood ratio test to predict the diagnoses (NC or SZ) of the held-out subjects. In particular, our test compares the likelihood of the test subject being generated from the control and the schizophrenic templates

$$\frac{P(\{D_n, B_n\} | \{\hat{A}_n, \hat{F}_n\}, \hat{\Theta}^*)}{P(\{D_n, B_n\} | \{\tilde{A}_n, \tilde{F}_n\}, \hat{\Theta}^*)} \stackrel{\text{'NC'}}{\geq} 1 \stackrel{\text{'SZ'}}{\leq} 1 \quad (21)$$

where  $\{\hat{A}_n, \hat{F}_n, \tilde{A}_n, \tilde{F}_n\}$  denotes the maximum *a posteriori* estimate for the latent templates when fitted to the training data, and  $\{D_n, B_n\}$  represents the observed DWI and fMRI data of a given test subject.

This process is repeated for each training-test set combination. In addition, we repeat the ten-fold cross validation 20 times using different groupings of subjects to evaluate the variability

<sup>1</sup>Our clinical dataset consists of 19 patients and 19 controls, which we divide into nine groups of four subjects and one group of two subjects. These groups specify the testing sets in our classification experiments. Since we infer differences between the populations, it is important to maintain equal numbers of control and schizophrenia subjects in each group to avoid biasing the solution towards one population.

of the results. For comparison, we perform ten-fold cross validation using the support vector machine (SVM) classifiers trained on the fMRI correlations and DWI tractography measures individually, as well as on the combined dataset.

### C. Baseline Methods

To evaluate the performance gain from combining fMRI and DWI data, we construct separate generative models for each modality. These individual models are depicted in Fig. 2. In these baseline models, we sever the connection between the anatomical connectivity templates and the fMRI data for each population.

Since the DWI data is independent of the latent functional connectivity, all parameters, random variables and data likelihoods remain unchanged for the DWI-only model [Fig. 2(a)].

The only modification in the fMRI-only model [Fig. 2(b)] involves the observed fMRI data. In particular, there are only three sets of likelihood parameters  $\{\mu, \sigma^2\}$  corresponding to the three latent functional connectivity states. Formally, we replace the likelihood in (4) with

$$P(B_{nj} | F_n; \{\mu, \sigma\}) = \prod_{k=-1}^1 \mathcal{N}(B_{nj}; \mu_k, \sigma_k^2)^{F_{nk}} \quad (22)$$

for the control subjects and

$$P(B_{nm} | \bar{F}_n; \{\mu, \sigma\}) = \prod_{k=-1}^1 \mathcal{N}(B_{nm}; \mu_k, \sigma_k^2)^{\bar{F}_{nk}} \quad (23)$$

for the schizophrenia population.

We employ EM solutions, similar to those in Section IV. The empirical probabilities of change  $\hat{\epsilon}_n^a, \hat{\epsilon}_n^f$  are computed according to (20) by replacing  $\hat{p}_{nl}$  with the posterior estimates of the appropriate model.

We perform permutation tests and cross validation using the DWI- and fMRI-specific models. These results allow us to evaluate the benefits of incorporating both imaging modalities in our analysis.

### D. Implementation Details

In this section we describe the optimization choices in our implementation of the EM algorithm. We concentrate on the

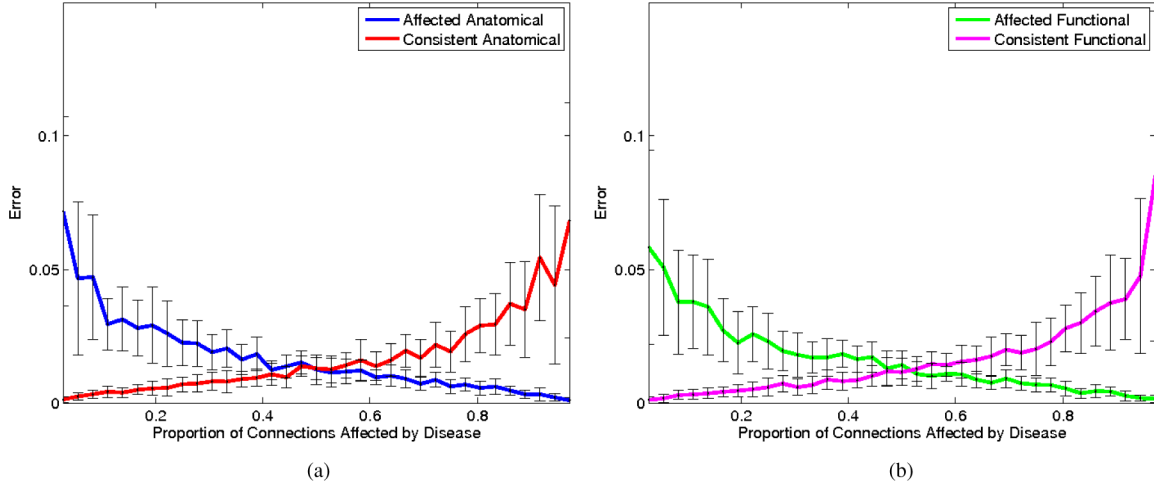


Fig. 3. Proportion of mislabeled connectivity relationships as a function of the proportion of latent connections affected by the disease. The bold lines represent the average error over 10 resamplings of the observed data  $\{B_{nj}, B_{nm}, D_{nj}, D_{nm}\}$ . The error bars represent one standard deviation from the mean. The likelihood parameterization is fixed at  $\mu_{00} = \mu_{10} = 0$ ,  $\mu_{01} = -\mu_{0,-1} = 0.1$ ,  $\mu_{11} = -\mu_{1,-1} = 0.15$ ,  $\chi_0 = 0.45$ ,  $\chi_1 = 0.55$ ,  $\rho_0 = 0.6$ , and  $\rho_1 = 0.4$ , which mimics the behavior of our clinical dataset. (a) Anatomical. (b) Functional.

model of population differences, as it is the primary focus of this work.

1) *Initialization*: Like many hill-climbing methods, the quality of our results depends on proper initialization. We initialize the model parameters  $\Theta = \{\pi, \mu, \sigma^2, \rho, \chi, \xi^2, \epsilon\}$  based on empirical measures computed from the clinical data. In particular, we randomly sample the initial values of  $\pi^a$ ,  $\pi_k^f$ ,  $\epsilon^a$  and  $\epsilon^f$  from the interval  $[0.3, 0.6]$ . This scheme produces values near the center of the parameter space. We set  $\sigma_{ik}^2$  and  $\xi_i^2$  to the variances (across all connections and subjects) of the fMRI correlations and the nonzero DWI data, respectively. We set  $\mu_{i0} = 0$ ,  $\mu_{i1} = \sigma_{i1}^2$  and  $\mu_{i,-1} = -\sigma_{i,-1}^2$ . This captures our assumptions about the effect of latent functional connectivity on fMRI correlations and reflects the fact that the relationship between latent anatomical connectivity and fMRI data is less clear. Finally, we randomly sample  $\chi_0$  and  $\chi_1$  from the range of DWI FA values and generate  $\rho_0 > \rho_1$ .

It is sufficient to initialize the model parameters. The algorithm starts with computing the joint posterior probability distribution (E-Step). Empirically, we find that the results are stable with respect to different initializations of the model parameters. Therefore, we run the algorithm five times to sample the probability space and select the maximum likelihood solution.

2) *Convergence and Run Time*: We ran the EM algorithm ten times using different subsets of subjects in each cross validation iteration. Convergence was based on the relative change in log-likelihood between iterations. On average, the algorithm converges in 87 iterations (E-step/M-step updates), and the average runtimes is 1.2 s per iteration. Thus, it requires on average 1.7 min to solve the model using EM. The iteration runtime scales linearly with the number of subjects. All simulations were performed using MATLAB on a single processor modern workstation.

## VI. EXPERIMENTAL RESULTS—SYNTHETIC DATA

We first evaluate the robustness and sensitivity of our algorithm using synthetic data. Throughout this section, we fix the

Gaussian variances  $\sigma_{1k}^2 = \sigma_{0k}^2 = \sigma^2 = 0.01$  and  $\xi_0^2 = \xi_1^2 = \xi^2 = 0.005$ , which corresponds to the parameter values estimated in the clinical dataset.

In all synthetic experiments, we fix the latent template and sample the observed data  $\{B_{nj}, B_{nm}, D_{nj}, D_{nm}\}$ , assuming 20 subjects in each population. We then infer the original latent templates from these noisy measurements. The error is computed as the proportion of connections for which the maximum *a posteriori* connectivity estimates do not match the ground truth templates. We repeat the experiment ten times to collect error statistics.

In the first experiment, we assume that the latent connectivity templates are similar for both populations. Specifically, the control templates have 180 pairwise connections for each of the six distinct values of latent connectivity templates  $\{A_n, F_n\}$  ( $N = 1080$ , comparable to the clinical dataset), and we randomly alter a small percentage of connections to obtain the schizophrenia templates. This mimics our clinical result that the changes induced by schizophrenia occur in a small yet spatially-distributed subset of connections.

We fix the fMRI likelihood parameters at  $\mu_{00} = \mu_{10} = 0$ ,  $\mu_{01} = -\mu_{0,-1} = 0.1$ , and  $\mu_{11} = -\mu_{1,-1} = 0.15$ . The resulting quantities  $|\mu_{01} - \mu_{0,-1}| = 0.2$  and  $|\mu_{11} - \mu_{1,-1}| = 0.3$ , which determine the separation between fMRI distributions for positive and negative latent functional connectivity, correspond to those estimated in the clinical dataset. Likewise, we fix the DWI likelihood parameters at  $\chi_0 = 0.45$ ,  $\chi_1 = 0.55$ ,  $\rho_0 = 0.6$ , and  $\rho_1 = 0.4$ . The quantity  $|\chi_1 - \chi_0| = 0.1$ , which influences the separation between DWI distributions for present and absent latent anatomical connectivity, is equivalent to that of the clinical dataset. The values for  $\rho_0$  and  $\rho_1$  are much closer than what we estimate from real data. Otherwise, we find that anatomical connectivity is perfectly recovered, and we cannot probe the model's behavior.

Fig. 3 shows the errors in determining the latent templates both for the consistent connections and for the connections affected by the disorder. The bold lines in Fig. 3 represent the av-

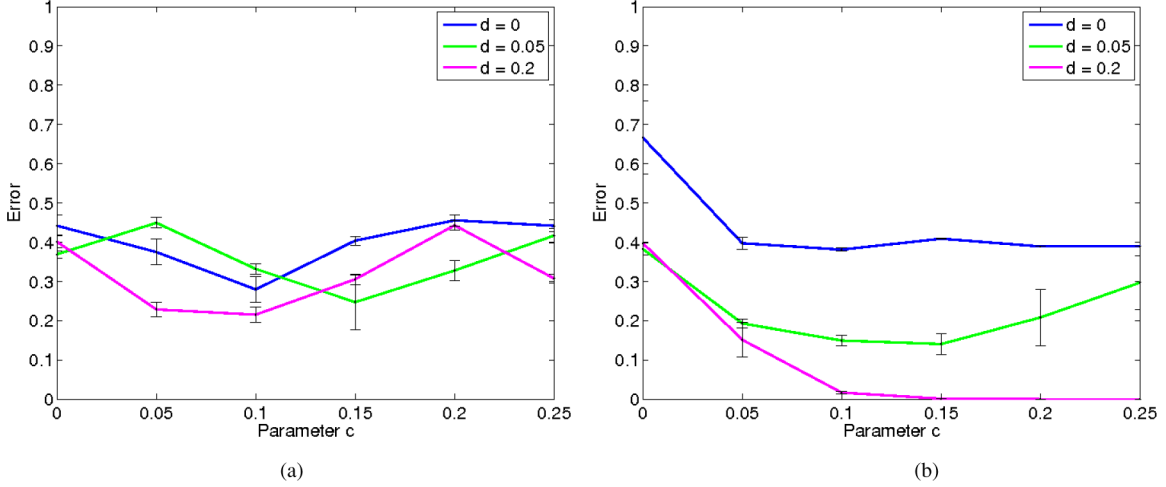


Fig. 4. Proportion of mislabeled connectivity relationships between the latent templates. The bold lines represent the average error over 10 resamplings of the observed data  $\{B_{nj}, B_{nm}, D_{nj}, D_{nm}\}$ . The error bars represent one standard deviation from the mean. The DWI likelihood parameterization is fixed at  $a = 0$  and  $b = 0.05$ . (a) Anatomical. (b) Functional.

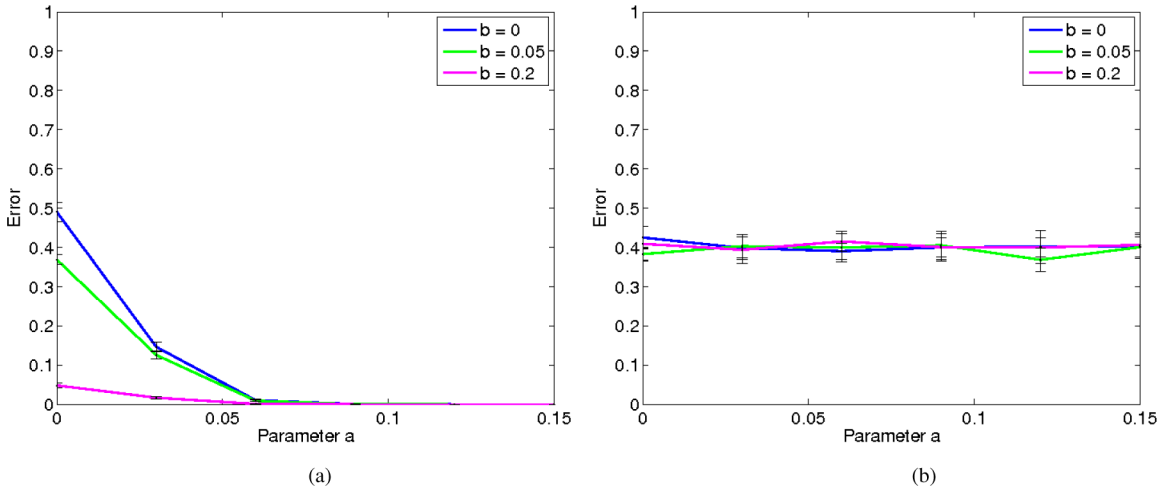


Fig. 5. Proportion of mislabeled connectivity relationships between the latent templates. The error is averaged over 10 resamplings of the data. The fMRI likelihood parameterization is fixed at  $c = 0$  and  $d = 0.05$ . (a) Anatomical. (b) Functional.

erage error over ten independent samples of the entire data set. The error bars represent one standard deviation. Clearly, when the proportion of affected connections is small, the algorithm has slightly more difficulty identifying them. Similarly, if the proportion of affected connections is large, the algorithm has difficulty recovering the consistent connections. For example, when 10% of connections are affected, the model correctly identifies 97% of them. But if 90% of the connections are affected, the model recovers 99% of them. The maximum error is less than 10%. This suggests that our algorithm can accurately fit the model, which is promising for the application to clinical data.

In the second experiment, we explore the breakdown points of our model. We consider the case when the DWI likelihood distributions provide little information about latent anatomical connectivity as well as the case when the fMRI likelihood distributions are nearly uninformative about latent anatomical and/or functional connectivity.

We parameterize the DWI model as follows:

$$\begin{aligned} \chi_0 &= 0.5 - a & \chi_1 &= 0.5 + a \\ \rho_0 &= 0.5 + b & \rho_1 &= 0.5 - b \end{aligned} \quad (24)$$

where  $a, b \geq 0$ . The parameter  $a$  controls the difference in DWI distributions for the two underlying anatomical connectivity values. The parameter  $b$  determines to how much more likely one is to find a DWI tract between two regions given a direct anatomical connection than if no connection is present.

We parameterize the Gaussian means for the fMRI model as follows:

$$\begin{aligned} \mu_{00} &= \mu_{10} = 0 \\ \mu_{01} &= c = -\mu_{0,-1} \\ \mu_{10} &= d = -\mu_{1,-1} \end{aligned} \quad (25)$$

where  $c, d \geq 0$ . The parameters  $c$  and  $d$  control the functional separation in the absence and presence of a latent anatomical connection, respectively. The quantity  $(d - c)$  relates to the effect anatomical connectivity has on the magnitude of fMRI correlations. This setup allows for adequate flexibility in manipulating the generative process while simultaneously reducing the number of free parameters to explore.

We assume a uniform distribution of latent connectivity values; the templates contain 30 pairwise connections for each of the 36 values of  $\{A_n, F_n, \bar{A}_n, \bar{F}_n\}$  ( $N = 1080$ ). We generate

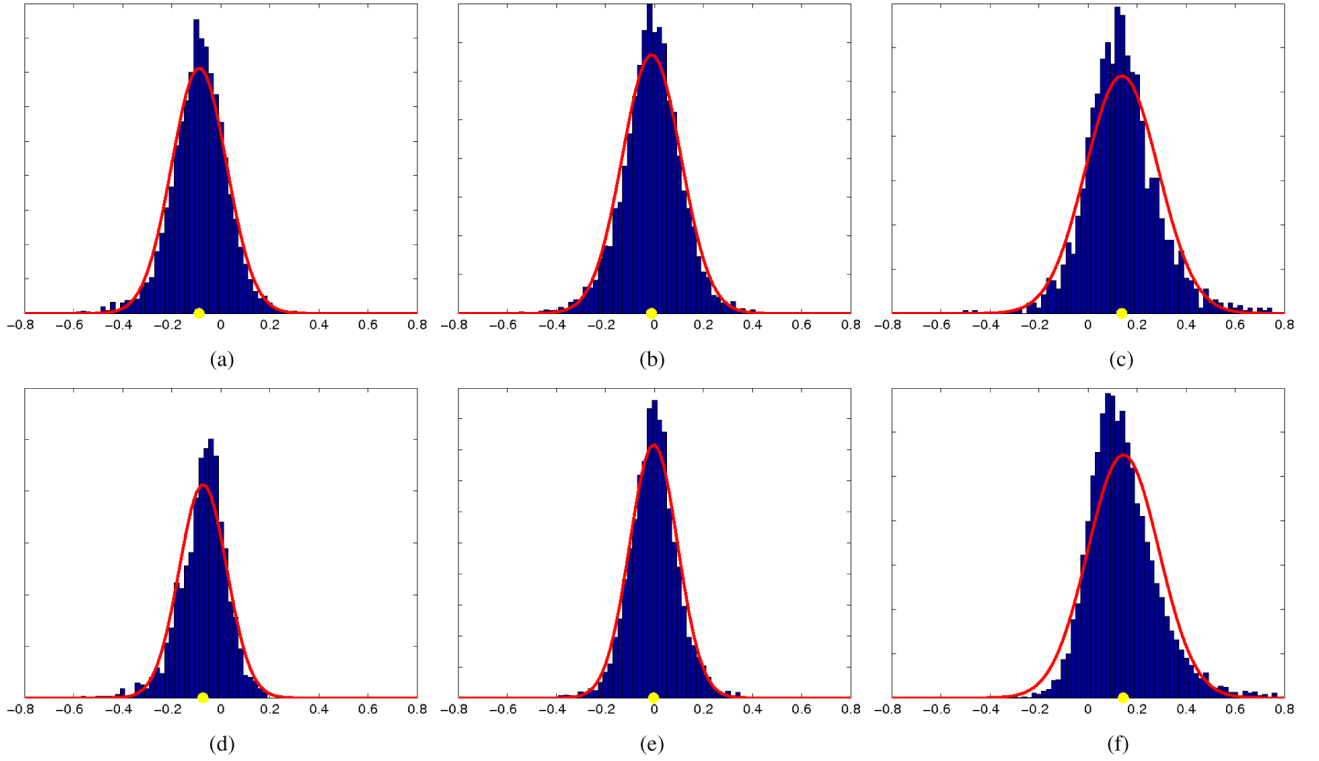


Fig. 6. Histograms of fMRI correlations based on estimated connectivity. Gaussian distributions that have been fitted to the data are overlaid in red. The yellow dots correspond to empirical means. (a)  $\hat{A}_n = 0, \hat{F}_n = -1$ . (b)  $\hat{A}_n = 0, \hat{F}_n = 0$ . (c)  $\hat{A}_n = 0, \hat{F}_n = 1$ . (d)  $\hat{A}_n = 1, \hat{F}_n = -1$ . (e)  $\hat{A}_n = 1, \hat{F}_n = 0$ . (f)  $\hat{A}_n = 1, \hat{F}_n = 1$ .

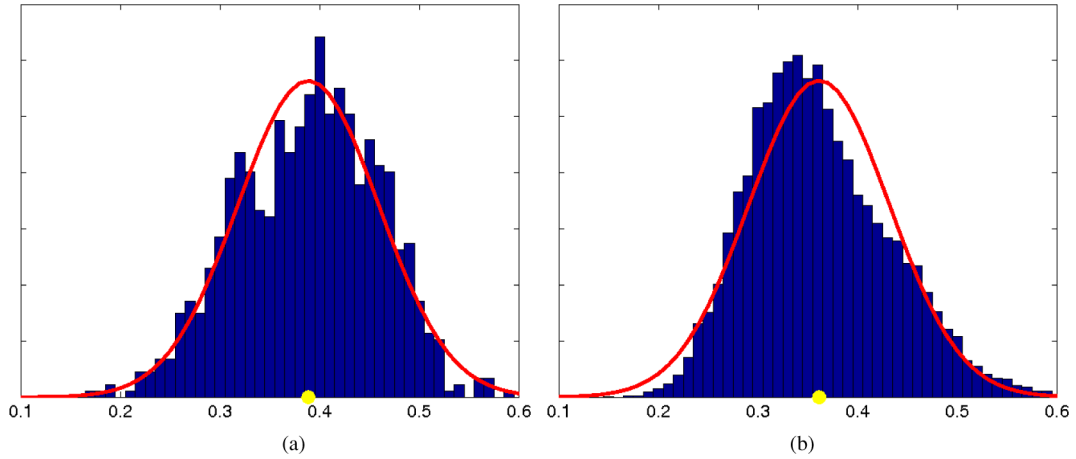


Fig. 7. Histograms of nonzero DWI data based on estimated anatomical connectivity. Gaussian distributions that have been fitted to the data are overlaid in red. The yellow dots correspond to empirical means. (a)  $\hat{A}_n = 0$ . (b)  $\hat{A}_n = 1$ .

20 subjects from each population and sweep the parameters in (24) and (25). For each parameter set, we generate data from the two-population model in Fig. 1(b) and solve for the latent connectivity. We repeat this procedure several times to ensure stability of the reported behavior.

First, we fix the DWI parameterization such that the probability of finding a tract is slightly greater than 0.5 given a latent anatomical connection ( $b = 0.05$ ), and such that there is no difference in DWI likelihood when a tract is observed ( $a = 0$ ). Fig. 4 reports the errors in predicting connectivity changes between the populations. We observe that as  $c, d$  increase from zero, the algorithm uses the fMRI data and the slight differ-

ence in DWI likelihood to estimate latent functional connectivity. Another interesting observation is the predictable dip in error in Fig. 4(a) when  $c, d \geq \sigma = 0.1$  and  $|d - c| \geq \sigma$ . In this case, the fMRI likelihoods based on positive/negative latent functional connectivity are simultaneously far from zero and distinct given the presence or absence of a latent anatomical pathway. The algorithm uses the first separation (far from zero) to identify latent functional connectivity and the second (based on anatomy) to infer latent anatomical connectivity.

Second, we fix the fMRI parameterization such that there is a slight separation between the mixture distributions given the presence of a latent anatomical connection ( $c = 0, d = 0.05$ ).

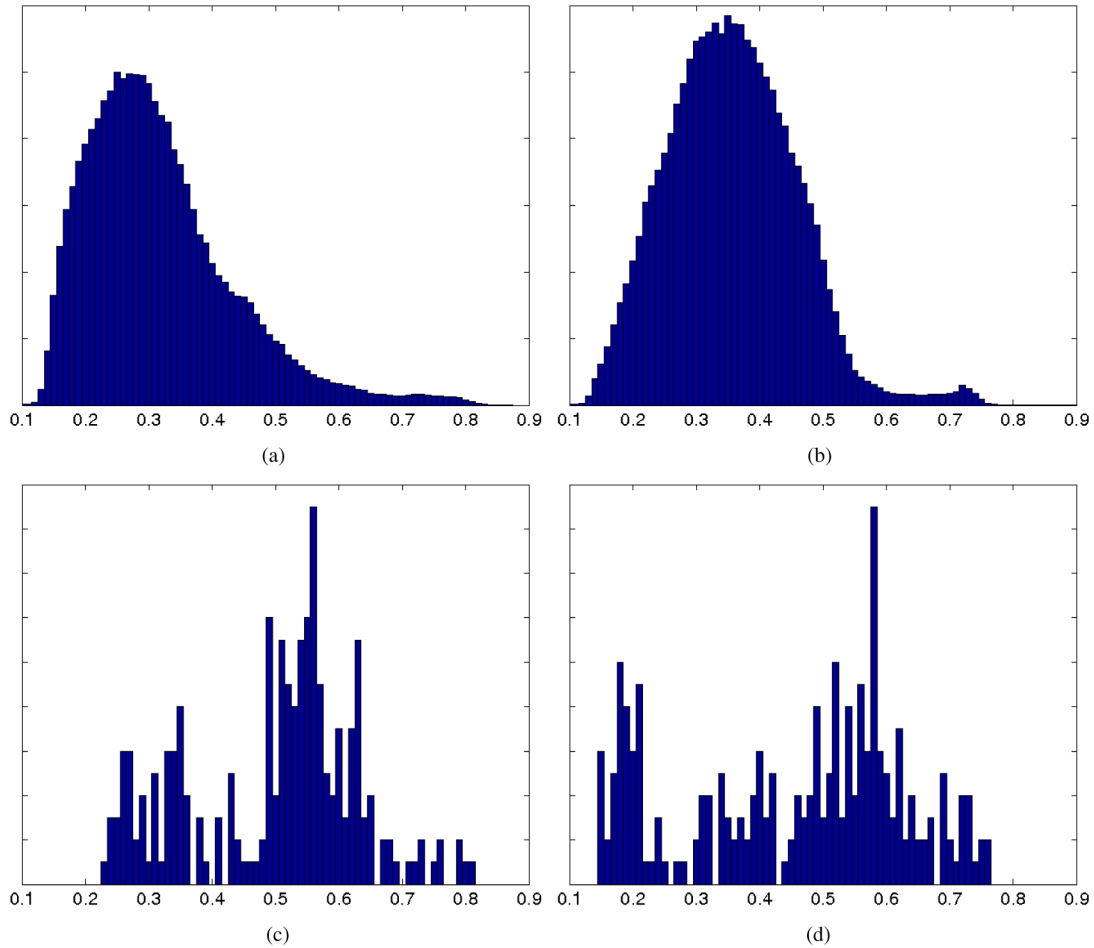


Fig. 8. Histograms of FA values along fibers for representative connections detected in all subjects [(a), (b)] and representative connections detected in a single subject [(c), (d)]. (a) R-Parahippocampal  $\leftrightarrow$  R-Hippocampus. (b) L-Posterior Cingulate  $\leftrightarrow$  L-Postcentral. (c) R-Cuneus  $\leftrightarrow$  L-Transverse Temporal Gyrus. (d) R-Rostral Anterior Cingulate  $\leftrightarrow$  R-Inferior Parietal.

TABLE III  
PARAMETERS OF THE JOINT MODEL IN FIG. 1(A). ANALYSIS IS PERFORMED SEPARATELY FOR CONTROL (NC)  
AND SCHIZOPHRENIC (SZ) POPULATIONS, AS WELL AS FOR THE ENTIRE DATASET (NC + SZ)

	$\pi_A$	$\pi_{F,-1}$	$\pi_{F0}$	$\pi_{F1}$	$\rho_0$	$\rho_1$	$\chi_0$	$\chi_1$	$\xi_0^2$	$\xi_1^2$
NC	0.37	0.45	0.38	0.17	0.66	0.10	0.42	0.34	0.005	0.003
SZ	0.38	0.44	0.42	0.14	0.68	0.11	0.41	0.34	0.005	0.003
NC+SZ	0.38	0.43	0.41	0.16	0.67	0.11	0.41	0.34	0.005	0.003

	$\mu_{0,-1}$	$\mu_{1,-1}$	$\mu_{00}$	$\mu_{10}$	$\mu_{01}$	$\mu_{11}$	$\sigma_{0,-1}^2$	$\sigma_{1,-1}^2$	$\sigma_{00}^2$	$\sigma_{10}^2$	$\sigma_{01}^2$	$\sigma_{11}^2$
NC	-0.062	-0.021	0.008	0.096	0.12	0.27	0.013	0.010	0.008	0.012	0.019	0.033
SZ	-0.083	-0.035	0.002	0.10	0.14	0.29	0.011	0.011	0.013	0.013	0.018	0.034
NC+SZ	-0.073	-0.027	0.002	0.10	0.12	0.28	0.012	0.011	0.012	0.012	0.018	0.034

Fig. 5 reports the errors in predicting the connectivity changes. An informative DWI likelihood (higher values of  $a, b$ ) allows us to correctly estimate the anatomical templates. However, it does not improve the estimates of latent functional connectivity. This is because our model does not include a direct link between the functional templates and the DWI data.

In summary, highly separable fMRI data allows us to estimate the functional templates and improves slightly our inference of latent anatomical connectivity. In contrast, highly separable DWI data produces accurate anatomical templates but does not improve the functional connectivity estimates. When

both datasets are informative, the algorithm recovers all the latent templates and model parameters.

## VII. EXPERIMENTAL RESULTS—CLINICAL DATA

### A. Image Acquisition and Preprocessing

We demonstrate our model on a study of 19 male patients with chronic schizophrenia and 19 healthy male controls. The control participants were group matched to the patients on age, handedness, parental socioeconomic status, and an estimated premorbid IQ. For each subject, an anatomical scan (SPGR,

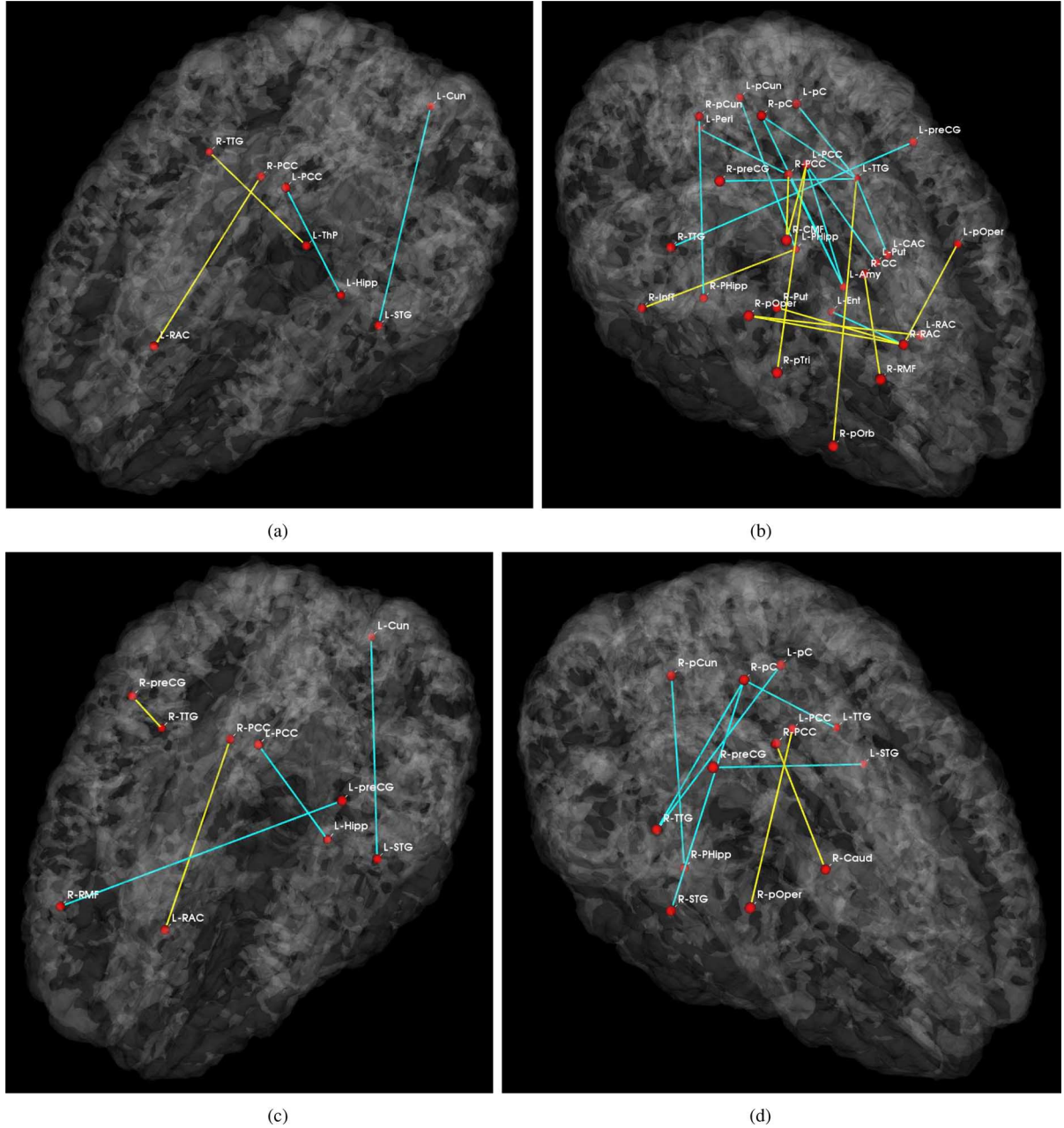


Fig. 9. Significant anatomical and functional connectivity differences ( $p < 0.05$  and  $\hat{e}_n^a, \hat{e}_n^f > 0.5$ ). Blue lines indicate higher connectivity in the control group; yellow lines indicate higher connectivity in the schizophrenia population. (a), (b) Derived from the joint DWI/fMRI model. (c) Significant anatomical connections from the DWI-only model. (d) Significant functional connections from the fMRI-only model. (a) Joint Model, Anatomical. (b) Joint Model, Functional. (c) DWI-only Model. (d) fMRI-only Model.

TR = 7.4 s, TE = 3 ms, FOV = 26 cm<sup>2</sup>, res = 1 mm<sup>3</sup>), a diffusion-weighted scan (EPI, TR = 17 s, TE = 78 ms, FOV = 24 cm, res = 1.66 × 1.66 × 1.7 mm, 51 gradient directions with  $b = 900$  s/mm<sup>2</sup>, 8 baseline scans with  $b = 0$  s/mm<sup>2</sup>) and a resting-state functional scan (EPI-BOLD, TR = 3 s, TE = 30 ms, FOV = 24 cm, res = 1.875 × 1.875 × 3 mm) were acquired using a 3T GE Echospeed system.

We segmented the structural images into 77 anatomical regions with Freesurfer [36]. The DWI data was corrected for eddy-current distortions using the FSL FLIRT algorithm [37]. A two-tensor tractography was used to estimate the white matter fibers [38]. We computed the DWI connectivity  $D_{nj}$  for connec-

tion  $n$  in subject  $j$  by averaging FA along all fibers that connect the corresponding regions. If no tracts were found,  $D_{nj}$  was set to zero.

We discarded the first five fMRI time points and performed motion correction by rigid body alignment and slice timing correction using FSL [37]. The data was spatially smoothed using a Gaussian filter, temporally low-pass filtered with 0.08 Hz cutoff, and motion corrected via linear regression. Finally, we removed global contributions to the time courses from the white matter, ventricles and the whole brain. We extracted the fMRI connectivity  $B_{nj}$  for connection  $n$  in subject  $j$  by computing Pearson correlation coefficients of the time courses between every pair

TABLE IV  
SIGNIFICANT ANATOMICAL AND FUNCTIONAL CONNECTIONS BASED ON THE JOINT GENERATIVE MODEL IN FIG. 1(B)

Anatomical Connections			
Region 1	Region 2	p	$\hat{\epsilon}_A^n$
L Posterior Cingulate (L-PCC)	L Hippocampus (L-Hipp)	0.0001	0.85
L Superior Temporal (L-STG)	L Cuneus (L-Cun)	0.0095	0.94
R Transverse Temporal (R-TTG)	L Thalamus-Proper (L-ThP)	0.031	0.99
R Posterior Cingulate (R-PCC)	L Rostral Anterior Cingulate (L-RAC)	0.042	0.97

Functional Connections			
Region 1	Region 2	p	$\hat{\epsilon}_F^n$
R Paracentral (R-pC)	L Transverse Temporal (L-TTG)	0.0001	0.88
R Pars Triangularis (R-pTri)	L Posterior Cingulate (L-PCC)	0.0001	0.79
R Posterior Cingulate (R-PCC)	L Amygdala (L-Amy)	0.0005	0.95
L Transverse Temporal (L-TTG)	L Paracentral (L-pC)	0.0005	0.54
L Posterior Cingulate (L-PCC)	L Amygdala (L-Amy)	0.0015	0.92
R Transverse Temporal (R-TTG)	L Precentral (L-preCG)	0.0035	0.71
R Precentral (R-preCG)	L Transverse Temporal (L-TTG)	0.0045	0.59
R Rostral Anterior Cingulate (R-RAC)	L Pars Opercularis (L-pOper)	0.0095	0.78
R Posterior Cingulate (R-PCC)	R Caudal Middle Frontal (R-CMF)	0.015	0.98
R Rostral Anterior Cingulate (R-RAC)	L Entorhinal Cortex (L-Ent)	0.015	0.64
R Precuneus (R-pCun)	R Parahippocampal (R-PHipp)	0.019	0.79
R Inferior Temporal (R-InfT)	L Parahippocampal (L-PHipp)	0.020	0.73
R Rostral Anterior Cingulate (R-RAC)	R Pars Opercularis (R-pOper)	0.0205	0.83
R Pars Opercularis (R-pOper)	L Rostral Anterior Cingulate (L-RAC)	0.021	0.99
R Pars Orbitalis (R-pOrb)	L Transverse Temporal (L-TTG)	0.023	0.69
R Rostral Anterior Cingulate (R-RAC)	R Putamen (R-Put)	0.025	0.73
R Rostral Middle Frontal (R-RMF)	R Corpus Callosum (R-CC)	0.031	0.81
L Transverse Temporal (L-TTG)	L Caudal Anterior Cingulate (L-CAC)	0.031	0.74
R Posterior Cingulate (R-PCC)	L Pericalcarine (L-Peri)	0.032	0.56
R Paracentral (R-pC)	L Amygdala (L-Amy)	0.036	0.54
L Posterior Cingulate (L-PCC)	L Putamen (L-Put)	0.043	0.95
R Caudal Middle Frontal (R-CMF)	L Posterior Cingulate (L-PCC)	0.044	0.88
L Precuneus (L-pCun)	L Parahippocampal (L-PHipp)	0.0465	0.52

of voxels in the two regions, applying the Fisher-r-to-z transform to each correlation (to enforce normality), and averaging these values. Since our anatomical regions are large, the correlation between the mean time courses of two regions shows poor correspondence with the distribution of voxel-wise correlations between them. Therefore, we believe our measure is more appropriate for fMRI correlations across subjects than the standard correlation of mean time courses.

To inject prior clinical knowledge, we preselected eight brain structures (corresponding to 16 regions) that are believed to play a role in schizophrenia: the superior temporal gyrus, rostral middle frontal gyrus, hippocampus, amygdala, posterior cingulate, rostral anterior cingulate, parahippocampal gyrus, and transverse temporal gyrus. We model only the 1096 ( $16 \times 76 - \binom{16}{2}$ ) unique pairwise connections between these ROIs and all other regions in the brain.

### B. Empirical Study of Data Distributions

In this section we present aggregate properties of our data, which motivate our choice of likelihood parameterization in Section III. We group both populations together, as the differences induced by schizophrenia are subtle and do not affect the global distributions.

We first fit the distributions of fMRI correlations and DWI FA values to our likelihood model in (3) and (4). Since we cannot access the latent connectivity  $A_n$  and  $F_n$ , we approximate these variables by working with average measures of the data across subjects. In particular, we threshold the proportion of subjects that exhibit white matter tracts between regions to estimate  $\hat{A}_n$ .

Similarly, we threshold the average fMRI correlations to estimate  $\hat{F}_n$ . We then analyze the distribution of DWI FA values and fMRI correlations across all connections in all subjects.

Fig. 6 depicts the histograms of fMRI correlations for all combinations of estimated latent connectivity. Fig. 7 illustrates histograms of the nonzero DWI values for the two types of anatomical connectivity. We have overlaid the fitted Gaussian distributions in each plot. The yellow dots correspond to empirical means. We observe that the variability in DWI and fMRI data across connections is across subjects are reasonably approximated using Gaussian distributions.

Fig. 7 also suggests that the average DWI measure is slightly higher for connections in which tractography identifies white matter tracts in only a few subjects ( $\hat{A}_n = 0$ ). We explore this phenomenon by considering the distribution of FA values along all fibers when (1) white matter tracts are detected in all subjects, and (2) white matter tracts are detected in only one subject. Our analysis considers the first scenario to represent a “true” anatomical connection and the second to be spurious fibers. Fig. 8 illustrates the histograms of two representative connections for each of the above cases.

Empirically, we find that the distributions of FA values along spurious fibers is more uniformly distributed across a broad range of values ( $FA \in [0.2, 0.8]$ ), whereas the distribution along true fibers is concentrated towards the lower end of this range ( $FA \in [0.3, 0.5]$ ). The average FA for a false-positive connection is higher than the FA for a correctly-identified connection.

There are several factors which may contribute to this phenomenon. In particular, since tractography is guided by the

TABLE V  
SIGNIFICANT ANATOMICAL (TOP) AND FUNCTIONAL (BOTTOM) CONNECTIONS BASED ON THE SINGLE-MODALITY GENERATIVE MODELS IN FIG. 2

Anatomical Connections			
Region 1	Region 2	p-value	$\hat{\epsilon}_n^a$
L Posterior Cingulate (L-PCC)	L Hippocampus (L-Hipp)	0.012	0.75
L Superior Temporal (L-STG)	L Cuneus (L-Cun)	0.029	0.79
R Posterior Cingulate (R-PCC)	L Rostral Anterior Cingulate (L-RAC)	0.030	0.99
R Rostral Middle Frontal (R-RMF)	L Precentral (L-preCG)	0.039	0.93
R Transverse Temporal (R-TTG)	R Precentral (R-preCG)	0.048	0.52

Functional Connections			
Region 1	Region 2	p-value	$\hat{\epsilon}_n^f$
R Pars Opercularis (R-pOper)	L Posterior Cingulate (L-PCC)	0.0009	0.97
R Paracentral (R-pC)	L Transverse Temporal (L-TTG)	0.0014	0.88
R Transverse Temporal (R-TTG)	R Paracentral (R-pC)	0.021	0.98
R Transverse Temporal (R-TTG)	L Paracentral (L-pC)	0.022	0.72
R Precentral (R-preCG)	L Superior Temporal (L-STG)	0.023	0.58
R Posterior Cingulate (R-PCC)	R Caudate (R-Caud)	0.027	0.55
R Precuneus (R-pCun)	R Parahippocampal (R-PHipp)	0.040	0.54
R Superior Temporal (R-STG)	R Paracentral (R-pC)	0.043	0.75

estimated tensors, perhaps the algorithm latches onto artificially high anisotropy in the DWI images to produce these erroneous tracts. Our two-tensor tractography algorithm [38] may also play a role. We fit one tensor along the main fiber bundle and use a second tensor to account for residual anisotropy. Our tractography algorithm computes only FA along the main fiber, which may impact the overall distribution.

### C. Joint Connectivity Model for the Clinical Data

We first fit the joint model in Fig. 1(a) to each population separately, as well as to the entire dataset. Table III reports the parameters of the three cases. We observe that the two solutions  $\{\pi, \mu, \sigma, \rho, \chi, \xi\}$  are largely consistent between the groups and for the combined case. This supports our hypothesis that population differences appear in the latent connectivities rather than in the data likelihood parameters.

Table III highlights some interesting properties of the data. For example,  $\mu_{0k} < \mu_{1k}$  for all  $k$ , which indicates that the presence of an anatomical connection between two regions increases the mean functional correlation. This result is consistent with prior work [4], [5]. Additionally,  $\chi_0 > \chi_1$  implies that false-positive white matter tracts have *higher* mean FA values than correctly-identified white matter tracts. This is consistent with our empirical evaluation of the data in Section VII-B.

### D. Population Study

Fig. 9 depicts the significantly different ( $\hat{\epsilon}_n > 0.5$ ) anatomical and functional connections identified by the algorithm. In this case, we identify connections with an uncorrected p-value of 0.05. Tables IV–V report the corresponding region pairs and significance values. Fig. 10 shows representative DWI fibers for the significant anatomical connections identified by the joint model. In each case, we display the corresponding tracts within a single subject from the population with *higher* connectivity. We note that the results of the joint model do not completely agree with those of the single-modality models.

Fig. 11 displays the connectivity differences while ensuring a false discovery rate of 0.05 [39]. We observe that few connections survive the stringent threshold. However, the uncorrected

results yield patterns that have previously been reported in the schizophrenia literature and are linked to clinical hypotheses regarding the disorder. For example, we observe that schizophrenia patients exhibit increased functional connectivity between the parietal/posterior cingulate region and the frontal lobe and reduced functional connectivity between the parietal/posterior cingulate region and the temporal lobe in Fig. 9. These results confirm the findings of functional abnormalities involving the default network and of widespread functional connectivity changes in schizophrenia [10], [22]. Likewise, the differences in anatomical connectivity are distributed across the brain.

In our experiments, we also observe consistency in parameter estimates across random subject relabelings in the permutation procedure (not shown). This suggests that the main effects of the label permutations are reflected in the latent connectivity rather than in the data likelihood.

Fig. 12 reports classification accuracy for the joint generative model, for the individual generative models, and for the SVM classifiers. Training accuracy is presented as validation that the model does learn discriminative features.

We acknowledge the low classification accuracy in Fig. 12 but emphasize that our model is not formulated for classification. In contrast, we aim to understand the interaction between fMRI and DWI data using a set of assumptions about connectivity and schizophrenia. Differences between the two populations are modeled through shifts in the likelihood parameters rather than by changes in specific fMRI and DWI values. Therefore, we do not expect our approach to achieve the performance of algorithms specifically tailored for classification, such as SVM. Rather, Fig. 12 illustrates three main points. First, the joint model achieves above-chance generalization accuracy. This suggests that the underlying connectivity might play a role in schizophrenia. Second, modeling anatomical and functional connectivity jointly yields predictive advantages over treating the fMRI and DWI data separately. Finally, the SVM accuracy is quite low. This underscores the well-documented challenge of finding robust functional and anatomical changes induced by schizophrenia [24], [40]. We note that much of the prior work on classification in schizophrenia did not rely on the modalities

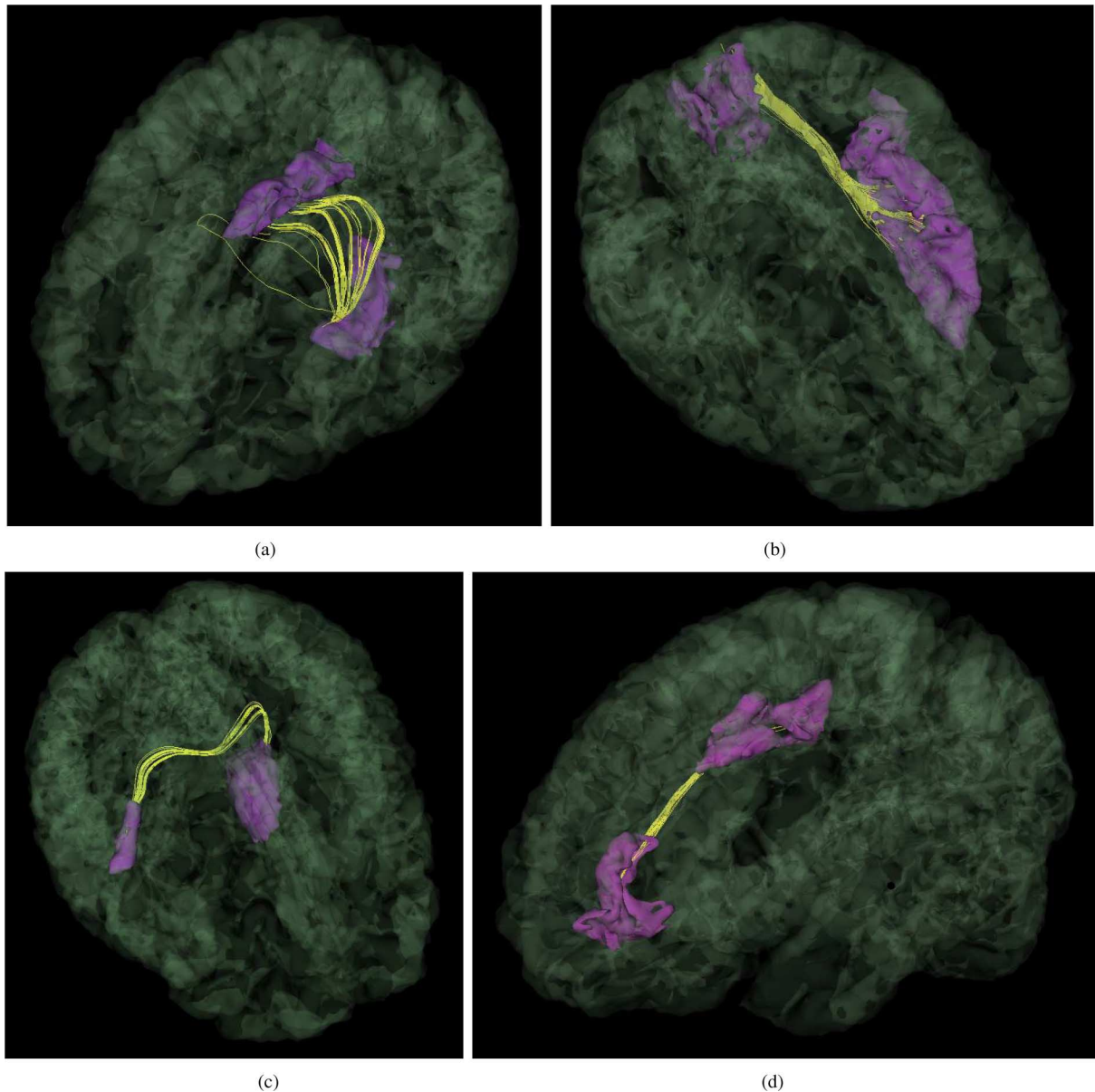


Fig. 10. Representative DWI fibers for each of the significant anatomical connections identified by the joint model in Table IV. The corresponding ROIs are displayed in pink; the fibers are depicted in yellow. (a) L-Posterior Cingulate  $\leftrightarrow$  L-Hippocampus. (b) L-Superior Temporal Gyrus  $\leftrightarrow$  L-Cuneus. (c) R-Transverse Temporal  $\leftrightarrow$  L-Thalamus Proper. (d) R-Posterior Cingulate  $\leftrightarrow$  R-Rostral Anterior Cingulate.

used in this paper. In particular, most reported classifiers consider volumetric changes found in T1 MRI [41] or activation patterns from task-based fMRI [42]. A few studies have focused on resting-state fMRI [26] or DTI tractography [43]. In all cases specialized classifiers were fine-tuned in order to obtain high accuracy.

## VIII. DISCUSSION

We formulate a generative model to infer changes in functional and anatomical connectivity induced by schizophrenia using both resting-state fMRI correlations and DWI tractography, and we present an algorithm for maximum likelihood estimation of the model parameters. We simultaneously obtain the joint posterior probability distribution of all the hidden variables, which allows us to identify population differences.

One interesting observation is the symmetry of functional connectivity differences across the hemispheres in Fig. 9(b) and (d). In particular, if a given functional connection shows significant differences between the populations, then functional connections involving those same regions in the opposite hemisphere tend to also be significant. This may arise from the well-documented symmetry found in resting-state fMRI correlations [34].

In contrast to functional connectivity, the model identifies few significant anatomical connections, only two of which are consistent between the algorithms. Moreover, the inter-hemispheric connections in Fig. 9(a) do not correspond to direct neural pathways within the brain. Rather, these connections arise from artifacts in the DWI images as well as from the behavior of our two-tensor tractography algorithm [38]. In particular, our algorithm recovers a much richer set of white matter fibers relative

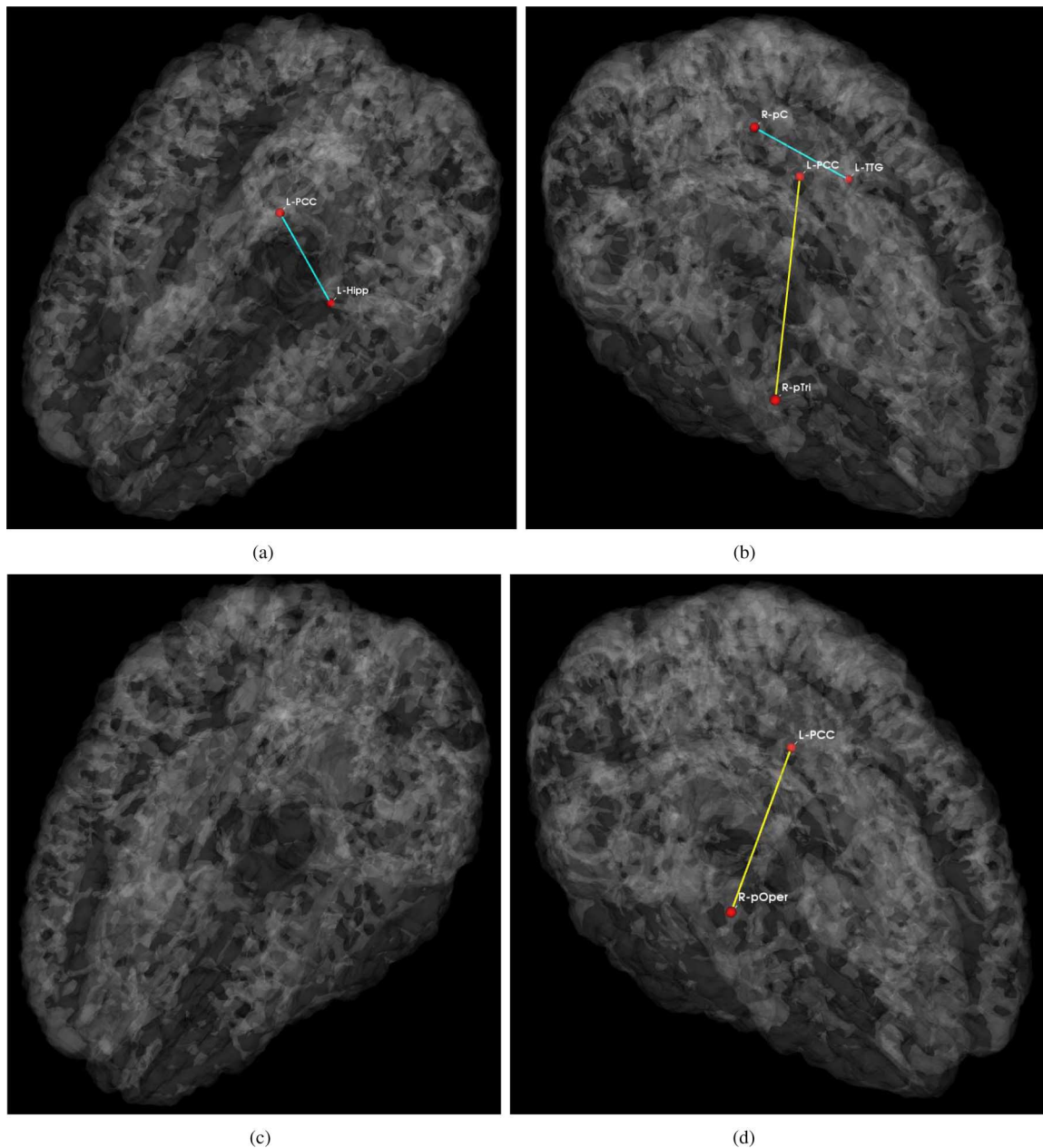


Fig. 11. Significant anatomical and functional connectivity differences with false discovery rate of 0.05. Blue lines indicate higher connectivity in the control group; yellow lines indicate higher connectivity in the schizophrenia population. (a), (b) Derived from the joint DWI/fMRI model. (c) Significant anatomical connections from the DWI-only model. (d) Significant functional connections from the fMRI-only model. (a) Joint Model, Anatomical. (b) Joint Model, Functional. (c) DWI-only Model. (d) fMRI-only Model.

to single-tensor methods. However, this set includes a larger number of false-positive tracts.

The results may also be influenced by our selection of regions. If the regions are too small, the variability in DWI tractography across subjects makes it difficult to infer the template anatomical connectivity and group-level parameters. However, larger regions smooth out important functional connectivity information. In this work, we rely on Brodman regions identified by Freesurfer. Brodman areas provide anatomically meaningful correspondences across subjects that roughly correspond to functional divisions within the brain. Moreover, these regions are large enough to ensure stable tractography results. We address the functional smoothing by computing *all* pairwise cor-

relations between voxels in two regions. This yields the entire distribution of functional connectivity. Presently, we select the mean of this distribution as a measure of functional correlation. However, other statistics can be incorporated as well (for example, mode of the distribution, variance, fitting to parameterized distributions). Finally, we emphasize that our framework applies readily to any set of ROIs that are defined consistently across subjects.

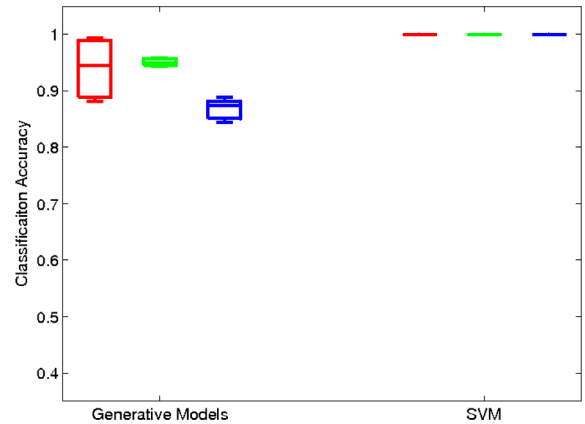
Despite the limited differences in anatomical connectivity, one justification for including the DWI data is the improved classification. We observe that combining fMRI and DWI data achieves better generalization accuracy than that of similar models built from one of these modalities. Additionally, most

significant functional connections obtained through the individual fMRI model are not consistent with those obtained via the joint models. Our experience with the algorithms suggests that the joint model focuses on the presence or absence of a white matter tract between two regions (rather than differences in FA) to determine latent anatomical connectivity. In particular, if several subjects exhibit a connection, then  $A_n$  is likely to be one; otherwise, it is likely to be zero. This is supported by results in synthetic data. Given a large difference in the probabilities of not finding a tract (e.g.,  $\rho_0 \approx 0.65$  and  $\rho_1 \approx 0.1$ , as estimated from the data), our algorithm correctly distinguishes latent anatomical connectivity, regardless of FA values. Once the anatomical connectivity pattern has been determined, the algorithm partitions the functional correlations into two groups. The mean functional correlation increases when there is a latent anatomical connection, which is reflected in the parameter estimates. The algorithms can reassign “borderline” connections based on the parameter/posterior estimates. We believe that this partition of fMRI correlations based on anatomical connectivity stabilizes the estimates of latent functional connectivity. This, in turn, allows the joint model to better explain differences between two populations.

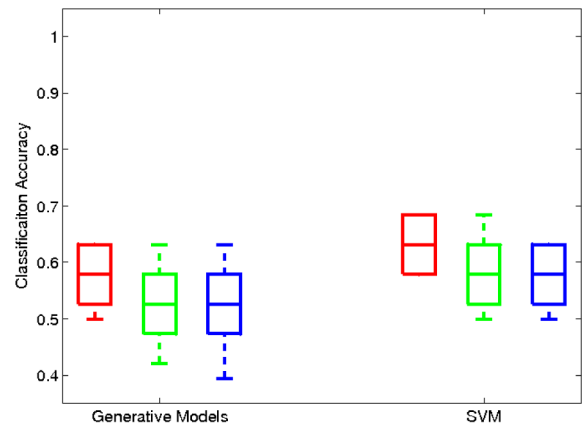
The significant (uncorrected) connections in Fig. 9 may reveal underlying neurological changes induced by the disease. We observe increased functional connectivity between the parietal/posterior cingulate region and the frontal lobe and reduced functional connectivity between the parietal/posterior cingulate region and the temporal lobe in the schizophrenia population.

When the results are corrected for multiple comparisons Fig. 11, the majority of functional connectivity differences disappear. However, the pattern of group differences seems to be preserved. Namely, reduced anatomical and functional connectivity in schizophrenia patients is limited to connections between the posterior cingulate cortex and the temporal lobe, while increased functional connectivity in schizophrenia appears between the posterior cingulate cortex and the medial/inferior frontal regions.

Increased connectivity between the default network and the medial frontal lobe, both at rest and during task, has been reported in schizophrenia [10], [44]. It is believed to interfere with perception of the external world through the misdirecting of attentional resources. Interestingly, decreased connectivity within the default network has been described as well [23], [31]. The later study reported decreased functional connectivity between the posterior cingulate gyrus and the hippocampus, which is consistent with our findings. The relationship between disruptions in functional connectivity and the integrity of the fornix has also been suggested. Similar to [23], our results reveal anatomical abnormalities within the two consistent anatomical connections (between the posterior cingulate and the hippocampus and between the superior temporal gyrus and the cuneus), which exhibits reduced anatomical connectivity in schizophrenia. We also observe a relationship between anatomical and functional connectivity disruptions within the posterior/temporal parts of the default network. Along with prior findings, our results suggest an inverse relationship between connectivity in the temporal and frontal parts of the default network. Such “anticorrelations” have been previously



(a)



(b)

Fig. 12. Training and testing accuracy of ten-fold cross validation using the joint generative model, the individual fMRI and DWI models and a linear SVM classifier. Red results are obtained using both modalities; green results are based only the DWI data; blue results are acquired from the fMRI data. The box denotes the upper and lower quartiles, the line indicates the median values, and the whiskers correspond to the 10th and 90th percentiles. (a) Training Accuracy. (b) Testing Accuracy.

described between the default and task-related networks, but never within the default network itself.

We recognize the limitations of our joint generative model, especially those related to its simplicity. For example, we consider only direct anatomical connections between two regions while ignoring multistage pathways. In reality, there is some interaction between connections, which can be used to extract anatomical and functional networks within the brain. We model latent connectivity via discrete random variables, which may marginalize subtle variations between groups, and we assume that all subject data are drawn from the same distribution, whereas the strength of fMRI correlations and FA values can vary across subjects. Finally, the relationship between the modalities is captured through the link from anatomical connectivity to fMRI correlations.

These choices are deliberate on our part. Since the interaction between resting-state fMRI correlations and DWI tractography is neither well understood nor well characterized, we avoid placing strong prior assumptions on the structural-functional relationship. Our goal at this stage is to model what we observe from the data using a simple, robust framework. Furthermore,

given the potentially large amounts of inter-subject variability and external noise, we intentionally simplify the model to reduce the number of parameters and avoid over-fitting. These limitations provide ample opportunities for future work.

## IX. CONCLUSION

We proposed a novel probabilistic framework that fuses information from resting-state fMRI correlations and DWI tractography to infer the differences between two populations. We show that the model captures variations in functional and anatomical connectivity induced by schizophrenia. In particular, we detect increased functional connectivity from the parietal lobe to the frontal lobe and decreased functional connectivity from the parietal lobe to the temporal lobe. Finally, we demonstrate the predictive power of our joint model through cross validation. These results establish the promise of our approach for combining multiple imaging modalities to better understand the brain.

## REFERENCES

- [1] R. L. Buckner and J. L. Vincent, "Unrest at rest: Default activity and spontaneous network correlations," *NeuroImage*, vol. 37, pp. 1091–1096, 2007.
- [2] M. D. Fox and M. E. Raichle, "Spontaneous fluctuations in brain activity observed with functional magnetic resonance imaging," *Nature*, vol. 8, pp. 700–711, 2007.
- [3] P. Basser and C. Pierpaoli, "Microstructural and physiological features of tissues elucidated by quantitative-diffusion-tensor MRI," *J. Magn. Reson.*, vol. 111, pp. 209–219, 1996.
- [4] C. J. Honey, O. Sporns, L. Cammoun, X. Gigandet, J. P. Thiran, R. Meuli, and P. Hagmann, "Predicting human resting-state functional connectivity from structural connectivity," *Proc. Nat. Acad. Sci.*, vol. 106, pp. 2035–2040, 2009.
- [5] M. A. Koch, D. G. Norris, and M. Hund-Georgiadis, "An investigation of functional and anatomical connectivity using magnetic resonance imaging," *NeuroImage*, vol. 16, pp. 241–250, 2002.
- [6] O. Sporns, G. Tononi, and G. M. Edelman, "Theoretical neuroanatomy: Relating anatomical and functional connectivity in graphs and cortical connection matrices," *Cerebral Cortex*, vol. 10, pp. 127–141, 2000.
- [7] C. J. Honey, R. Kotter, M. Breakspear, and O. Sporns, "Network structure of cerebral cortex shapes functional connectivity on multiple time scales," *Proc. Nat. Acad. Sci.*, vol. 104, pp. 10 240–10 245, 2007.
- [8] M. Ke, X. Huang, H. Shen, Z. Zhou, X. Chen, and D. Hu, "Combined analysis for resting state fMRI and DTI data reveals abnormal development of function-structure in early-onset schizophrenia," *LNAI*, vol. 5009, pp. 628–635, 2008.
- [9] Y. Zhou, N. Shu, Y. Liu, M. Song, Y. Hao, H. Liu, C. Yu, Z. Liu, and T. Jiang, "Altered resting-state functional connectivity and anatomical connectivity of hippocampus in schizophrenia," *Schizophrenia Res.*, vol. 100, pp. 120–132, 2008.
- [10] S. Gabrieli-Whitfield, H. W. Thermenos, Z. Milanovic, M. T. Tsuang, S. V. Faraone, R. W. McCarley, M. E. Shenton, A. I. Green, A. Nieto-Castanon, P. LaViolette, J. Wojcik, J. D. Gabrieli, and L. J. Seidman, *Hyperactivity and Hyperconnectivity of the Default Network in Schizophrenia and in First-Degree Relatives of Persons With Schizophrenia*. Washington, DC: Nat. Acad. Sci., 2009, pp. 1279–1284.
- [11] J. Burns, D. Job, M. E. Bastin, H. Whalley, T. MacGillivray, E. C. Johnstone, and S. M. Lawrie, "Structural disconnectivity in schizophrenia: A diffusion tensor magnetic resonance imaging study," *Br. J. Psychiatry*, vol. 182, pp. 439–443, 2003.
- [12] A. Venkataraman, Y. Rathi, M. Kubicki, C.-F. Westin, and P. Golland, "Joint generative model for fMRI/DWI and its application to population studies," in *MICCAI: Int. Conf. Med. Image Computing Computer Assist. Intervent.*, 2010, vol. 13, pp. 191–199.
- [13] K. Friston, A. Holmes, K. Worsley, J.-P. Poline, C. Frith, and R. Frackowiak, "Statistical parametric maps in functional imaging: A general linear approach," *Human Brain Mapp.*, vol. 2, pp. 189–210, 1995.
- [14] M. Guye, G. J. Parker, M. Symms, P. Boulby, C. A. Wheeler-Kingshott, A. Salek-Haddadi, G. J. Barker, and J. S. Duncan, "Combined functional MRI and tractography to demonstrate the connectivity of the human primary motor cortex in vivo," *NeuroImage*, vol. 19, pp. 1349–1360, 2003.
- [15] R. F. Dougherty, M. Ben-Shachar, R. Bammer, A. A. Brewer, and B. A. Wandell, "Functional organization of occipital-callosal fiber tracts," *Proc. Nat. Acad. Sci.*, vol. 102, pp. 7350–7355, 2005.
- [16] H. W. Powell, G. J. Parker, D. C. Alexander, M. R. Symms, P. A. Boulby, C. A. Wheeler-Kingshott, G. J. Barker, U. Noppeney, M. J. Koepp, and J. S. Duncan, "Hemispheric asymmetries in language-related pathways: A combined functional MRI and tractography study," *NeuroImage*, vol. 32, pp. 388–399, 2006.
- [17] H. Johansen-Berg, T. E. Behrens, M. D. Robson, I. Drobnjak, M. F. Rushworth, J. M. Brady, S. M. Smith, D. J. Higham, and P. M. Matthews, "Changes in connectivity profiles define functionally distinct regions in human medial frontal cortex," *Proc. Nat. Acad. Sci.*, vol. 101, pp. 13 335–13 340, 2004.
- [18] A. T. Toosy, O. Ciccarelli, G. J. Parker, C. A. Wheeler-Kingshott, D. H. Miller, and A. J. Thompson, "Characterizing function-structure relationships in the human visual system with functional MRI and diffusion tensor imaging," *NeuroImage*, vol. 21, pp. 1452–1463, 2004.
- [19] E. Rykhlevskaia, G. Gratton, and M. Fabiani, "Combining structural and functional neuroimaging data for studying brain connectivity: A review," *Psychophysiology*, vol. 45, pp. 173–187, 2008.
- [20] M. D. Greicius *et al.*, "Resting-state functional connectivity in the default mode network," *Cerebral Cortex*, vol. 19, pp. 72–78, 2009.
- [21] M. D. Greicius, B. H. Flores, V. Menon, G. H. Glover, H. B. Solvason, H. Kenna, A. L. Reiss, and A. F. Schatzberg, "Resting-state functional connectivity in major depression: Abnormally increased contributions from subgenual cingulate cortex and thalamus," *Biol. Psychiatry*, vol. 62, pp. 429–437, 2007.
- [22] M. Liang, Y. Zhou, T. Jiang, Z. Liu, L. Tian, H. Liu, and Y. Hao, "Widespread functional disconnectivity in schizophrenia with resting-state functional magnetic resonance imaging," *NeuroReport Brain Imag.*, vol. 17, pp. 209–213, 2006.
- [23] Y. Zhou, M. Liang, T. Jiang, L. Tian, Y. Liu, Z. Liu, H. Liu, and F. Kuang, "Functional disconnectivity of the dorsolateral prefrontal cortex in first-episode schizophrenia using resting-state fMRI," *Neuro Lett.*, vol. 417, pp. 297–302, 2007.
- [24] M. Kubicki, R. McCarley, C.-F. Westin, H.-J. Park, S. Maier, R. Kikinis, F. A. Jolesz, and M. E. Shenton, "A review of diffusion tensor imaging studies in schizophrenia," *J. Psychiatric Res.*, vol. 41, pp. 15–30, 2007.
- [25] M. J. Jafri, G. D. Pearlson, M. Stevens, and V. D. Calhoun, "A method for functional network connectivity among spatially independent resting-state components in schizophrenia," *NeuroImage*, vol. 39, pp. 1666–1681, 2008.
- [26] M. Jafri and V. Calhoun, "Functional classification of schizophrenia using feed forward neural networks," in *International Conference of the IEEE Engineering in Medicine and Biology Society*, 2006, pp. 6631–6634.
- [27] K. J. Friston and C. D. Frith, "Schizophrenia: A disconnection syndrome?," *Clinical Neuroscience*, vol. 3, pp. 89–97, 1995.
- [28] R. Tandon, M. S. Keshavan, and H. A. Nasrallah, "Schizophrenia, 'just the facts': What we know in 2008, Part 1: Overview," *Schizophrenia Res.*, vol. 100, pp. 4–19, 2008.
- [29] M. E. Shenton, C. C. Dickey, M. Frumin, and R. W. McCarley, "A review of MRI findings in schizophrenia," *Schizophrenia Res.*, vol. 49, pp. 1–52, 2001.
- [30] R. L. Mitchell, R. Elliott, and P. W. Woodruff, "fMRI and cognitive dysfunction in schizophrenia," *TRENDS Cognitive Sci.*, vol. 5, pp. 71–81, 2001.
- [31] R. L. Bluhm, J. Miller, R. A. Lanius, E. A. Osuch, K. Boksman, R. W. Neufeld, J. Théberge, B. Schaefer, and P. Williamson, "Spontaneous low-frequency fluctuations in the bold signal in schizophrenic patients: Abnormalities in the default network," *Schizophrenia Bull.*, pp. 1–9, 2007.
- [32] R. L. Buckner, J. R. Andrews-Hanna, and D. L. Schacter, "The brain's default network anatomy, function, and relevance to disease," *Ann. NY Acad. Sci.*, vol. 1124, pp. 1–38, 2008.
- [33] A. Konrad and G. Winterer, "Disturbed structural connectivity in schizophrenia—Primary factor in pathology or epiphenomenon," *Schizophrenia Bull.*, vol. 34, pp. 72–92, 2008.

- [34] K. V. Dijk, T. Hedden, A. Venkataraman, K. Evans, S. Lazar, and R. Buckner, "Intrinsic functional connectivity as a tool for human connectomics: Theory, properties and optimization," *J. Neurophysiol.*, vol. 103, pp. 297–321, 2010.
- [35] A. Dempster, N. M. Laird, and D. B. Rubin, "Maximum likelihood from incomplete data via the EM algorithm," *J. R. Stat. Soc.*, vol. 39, pp. 1–38, 1977.
- [36] B. Fischl, D. H. Salat, A. J. van der Kouwe, N. Makris, F. Ségonne, B. T. Quinn, and A. M. Dale, "Sequence-independent segmentation of magnetic resonance images," *NeuroImage*, vol. 23, pp. 69–84, 2004.
- [37] S. M. Smith, M. Jenkinson, M. W. Woolrich, C. F. Beckmann, T. E. Behrens, H. Johansen-Bern, P. R. Bannister, M. D. Luca, I. Drobnjak, D. E. Flitney, R. K. Niazy, J. Saunders, J. Vickers, Y. Zhang, N. D. Stefano, J. M. Brady, and P. M. Matthews, "Advances in functional and structural MR image analysis and implementation as FSL," *NeuroImage*, vol. 23, pp. 208–219, 2004.
- [38] J. G. Malcolm, M. E. Shenton, and Y. Rathi, "Neural tractography using an unscented Kalman filter," in *Int. Conf. Inf. Process. Med. Imag.*, 2009, vol. 21, pp. 126–138.
- [39] Y. Benjamini and Y. Hochberg, "Controlling the false discovery rate: A practical and powerful approach to multiple testing," *J. R. Stat. Soc., Ser. B (Methodological)*, vol. 57, pp. 125–133, 1995.
- [40] O. Demirci, V. Clark, V. Magnotta, N. Andreasen, J. Lauriello, K. Keihl, G. Pearlson, and V. Calhoun, "A review of challenges in the use of fMRI for disease classification/characterization and a projection pursuit application from a multi-site fMRI schizophrenia study," *Brain Imag. Behav.*, vol. 2, pp. 207–226, 2008.
- [41] Y. Fan, R. Gur, R. Gur, X. Wu, D. Shen, M. Calkins, and C. Davatzikos, "Unaffected family members and schizophrenia patients share brain structure patterns: A high-dimensional pattern classification study," *Biol. Psychiatry*, vol. 63, pp. 118–124, 2008.
- [42] J. Ford, H. Farid, F. Makedon, L. Flashman, T. McAllister, V. Megalooikonomou, and A. Saykin, "Patient classification of fMRI activation maps," in *MICCAI: Int. Conf. Med. Image Computing Computer Assist. Intervent.*, 2003, vol. 6, pp. 58–65.
- [43] V. Mohan, G. Sundaramoorthi, M. Kubicki, T. Douglas, and A. Tannenbaum, "Population analysis of the cingulum bundle using the tubular surface model for schizophrenia detection," *Med. Imag. 2010: Computer-Aided Diagnosis*, vol. 7624, 2010.
- [44] Y. Zhou, M. Liang, T. Jiang, L. Tian, Y. Liu, Z. Liu, H. Liu, and F. Kuang, "Functional dysconnectivity of the dorsolateral prefrontal cortex in first-episode schizophrenia using resting-state fMRI," *Neurosci. Lett.*, vol. 417, pp. 297–302, 2007.